Energy Reports 6 (2020) 2956–2972

Contents lists available at ScienceDirect

Energy Reports

journal homepage: www.elsevier.com/locate/egyr

Correction of cavitation with thermodynamic effect for a diaphragm pump in organic Rankine cycle systems

Wenguang Li, Andrew Mckeown, Zhibin Yu *

School of Engineering, University of Glasgow, Glasgow, G12 8QQ, UK

ARTICLE INFO

Article history:
Received 30 July 2020
Received in revised form 23 September 2020
Accepted 13 October 2020
Available online xxxx

Keywords:
Diaphragm pump
Cavitation
Thermodynamic effect
Organic Rankine cycle
Organic fluid
Net positive suction head required

ABSTRACT

Diaphragm pumps are a sort of leakage-proof reciprocating pumps with low flow rate but high head and better efficiency, and can potentially find their applications in organic Rankine cycle (ORC) systems as the feed-pump of organic fluid to the evaporator. A diaphragm pump in an ORC system may suffer from cavitation in the pump suction chamber inevitably when the pump delivers an organic fluid. However, the cavitation performance of the pump has been a little known for organic fluids so far. In the article, the performance of a specific diaphragm pump was determined based on the existing performance charts provided by the pump manufactory in terms of pump rotating speed and inlet liquid pressure for cold water. The net positive suction head required (NPSHr) was predicted by involving thermodynamic effect in cavitation when the pump feeds the organic liquid R245fa to the evaporator in an ORC system at 480rpm rotational speed. The net positive suction head available (NPSHa) was calculated at 100 kPa and 141 kPa inlet liquid pressures, and the corresponding cavitation safety margins were addressed. The subcooling for the NPSHr and NPSHa as well as the safety margin were figured out. Two one-dimensional (1D) mechanical models for motion of the suction valve were built and solved at 480rpm and 100 kPa and 141 kPa inlet pressures. A preliminary experiment was performed to verify the analytical results. It turned out that the NPSHr is reduced to 2.02m from 3.02m NPSHr of cold water due to the thermodynamic effect in cavitation, and the corresponding subcooling is lowered to 8.28 °C from 12.38 °C. 100 kPa but 141 kPa inlet pressure can result in cavitation in the pump. The 1D mechanical models are subject to a rough spatial resolution for the flow field in the suction chamber, hence three-dimensional(3D) numerical simulations of the flow field are desirable.

1. Introduction

Cavitation is a phenomenon whereby a proportion of liquid suffers from vaporization when the absolute pressure in a local fluid field is as low as the saturated vapour pressure in a fluid flow system. When the cavitation occurs in a pump, the pump will experience performance degradation, noise, vibration and even potential mechanical damage. To prevent a pump from cavitation, a sufficient large net positive suction head (NPSH), or net positive suction head available (NPSHa), which is the total energy of a fluid at the pump inlet minus the saturated vapour pressure at the pump operating temperature, is required. In other words, a pump has a net positive suction head required (NPSHr), which is the total energy loss and pressure drop from the pump inlet to the impeller or pumping chamber. To avoid cavitation, NPSHa must be higher than NPSHr with a safety margin for a pump. Usually, for a rotodynamic pump, the NPSHa at the pump head has dropped off by 3% in comparison with the head under non-cavitation condition is redeemed as the NPSHr of the pump. For a positive displacement pump, however, the counterpart at the pump mean flow rate has dropped off by 3% compared with the flow rate under non-cavitation condition is considered as the NPSHr of that pump

Organic Rankine cycle (ORC) is the thermodynamic cycle which employs organic fluids are a sort of fluids with high molecular masses and low atmospheric boiling points. The first solar driven ORC system was created in 1960's by Israeli physicists. Since then, this power generation technique has found applications in heat recovery from lower temperature sources, namely biomass combustion, industrial waste heat, geothermal heat and so on. ORC research field is now well developed and an extensive body of ORC literature has been published. The latest reviews of ORC can be found in Chen et al. (2010), Quoilin et al. (2013), Tchanche et al. (2014), Colonna et al. (2015) and Park et al. (2018) to name a few.

Even though a laboratory-scale pumpless ORC system was proposed by swapping hot and cold sources periodically (Yamada et al., 2013; Gao et al., 2015), or the system was operated by using

* Corresponding author.
E-mail address: Zhibin.yu@glasgow.ac.uk (Z. Yu).

https://doi.org/10.1016/j.egyr.2020.10.013

thermofluidic feed pumps (Richardson, 2016; Shu et al., 2018), in practical terms the addition of a mechanical feed pump remains convenient particularly for large-scale ORC systems (Usman et al., 2015; Rahbar et al., 2015). As a result, various studies have been devoted to different aspects of the ORC pump.

The hydraulic and cavitation performance of a variable-stroke axial piston swashplate pump was measured in a testing loop with organic fluids R11 and R113 at 1750–3000 rpm rotating speeds and 20–80 °C temperatures (Bollina, 1984). The flow rate versus NPSHa curves for R11 and R113 were obtained. Since the cavitation performance of the pump for water was not tested, one was unable to figure out the difference in cavitation performance between the organic fluids and the water. The hydraulic performance of a positive displacement pump with sliding vanes was tested with R11 and R113 and their blend mixture for ORC systems at different rotating speeds and pressure differences (Bala et al., 1985). The quantity of vapour in the pump with R11 was greater than R113. A positive displacement pump with sliding vanes was tested with organic fluid R236fa at 700–1200 rpm rotating speeds and 17–24 °C temperatures (Bianchi et al., 2016). Unfortunately, the pump total efficiency is 35% only. The pumping work in ORC systems was estimated analytically for 18 kinds of organic fluids (Borsukiewicz-Gozdur, 2013), and the work increases with decreasing critical temperature of the fluids. The performance match between expander (a scroll compressor in reverse mode) and feed pump (a reciprocating piston pump) was investigated experimentally by using organic fluid R123 in Yang et al. (2015), and the expander can operate in the whole range of torque when the pump rotational speed is less than 600 rpm (10 Hz) or the expander generates a smaller torque only due to cavitation in the pump caused from a faster rotational speed. To avoid the cavitation the liquid should be subject to a 20 °C subcooling at the pump inlet. The subcooling is the difference in the boiling temperature of a liquid from its actual temperature at the same pressure. In comparison, the subcooling is 13 °C for a reciprocating plunger pump when feeding R245fa in an ORC system (Chang et al., 2015).

The performance parameters of the diaphragm pumps, such as Hydra-Cell G03X, G10X, were measured in a simplified ORC system (without expander of turbine) with organic fluids R134a, R404 and a mixture NH_3/H_2O, respectively (Landelle et al., 2015, 2017). The measured Hydra-Cell G03X pump volumetric efficiency–pressure curve of R134a differs significantly from that of water provided by the pump manufacture. The NPSHr was 0.24 bar for R134a at nominal rotational speed, compared with 0.36 bar for water in the pump data sheet provided by the pump manufacture. The corresponding tested subcooling was 4.4 °C for that pump. For organic fluid R245fa, an empirical model was proposed to predict the non-cavitation performance of the diaphragm pump of Hydra-Cell D/G-10X pump in an ORC system (D'Amico et al., 2018).

The overall performance of three pumps such as multistage centrifugal pump, diaphragm pump, and roto-jet pump was measured in thermal test rig loop of R245fa in various rotational speeds (Yang et al., 2018). Three pumps share about the same overall efficiency, and the diaphragm pump is more suitable to a lower heat capacity ORC system, and the centrifugal pump is better for a higher heat capacity system, but the roto-jet pump is in between. The performance of a multistage centrifugal pump was tested in a thermal test rig loop of R245fa under various condensation conditions, and the condensation conditions affect the performance of the multistage centrifugal pump slightly (Yang et al., 2019). The ORC system was tested when a reciprocating plunger pump and a centrifugal pump were installed, respectively. The system with the plunger pump is more efficient 12.51% than that with the centrifugal pump, and the plunger pump is more suitable to the ORC system studied (Wang et al., 2020). A peripheral pump model PK70 with 0.8 kg/s flow rate and 65 m head was tested in transporting HEF-7100 organic fluid in an ORC system with regeneration and without regeneration in (17–57) °C and 2900 r/min Kaczmarczyk et al. (2016). The pump head is 41–43 m at (0.16–0.17) kg/s mass flow, and HEF-7100 vapour occurs in the pump. Transient CFD approach is launched to analyse fluid dynamics of the pumping system of a regenerative lab-scale micro-ORC system consisting of the liquid receiver, pipeline, external gear pump and mass flow meter (Casari et al., 2019), and the results indicated that cavitation phenomenon affects the pump and ORC system operation.

Based on the outcomes of the distinct studies mentioned above, most of them were focused on the pump overall performance to match a particular ORC system and cavitation in an ORC system can influence pump and system operation. The pump cavitation has been less known, especially in terms of thermodynamic effect in cavitation of organic fluids so far.

In the article, the cavitation performance of a diaphragm pump of G20-E model when delivering the organic fluid R245fa was investigated analytically. A NPSHr correction method was formulated based on the thermodynamic effect in cavitation, and one-dimensional(1D) motion of the suction valve was simulated numerically by using two mechanical models proposed to identify the cavitation at 100 kPa and 141 kPa pump inlet pressures along with preliminary experiments. The NPSHa values at those inlet pressures were calculated and cavitation safety margin was addressed, the subcooling for the NPSHr, NPSHa and safety margin was worked out. The study will provide useful information for both selection and safe operation of the diaphragm pump in ORC systems.

2. Pump performance determination

2.1. Pump operational parameter extraction

A positive displacement diaphragm pump of G20-E model, manufactured by Wanner Engineering Inc, was selected to circulate organic fluid R245fa in a small-scale ORC system, as shown in Fig. 1a. The pump liquid end structure is sketched conceptively in Fig. 1b. The pump mainly consists of eight mechanical components: drive crank, connecting rod, piston, piston casing, diaphragm, inlet and discharge valves and valve housing. The diaphragm is driven by the piston via the hydraulic oil in the left chamber of the diaphragm. When the piston moves to the left, the volume of the chamber between the two valves and the diaphragm is expanded, the pressure in the chamber is depressed, the suction valve is opened and the discharge valve is closed, drawing liquid into the chamber. In this period of time, the pump is in suction stroke. As the piston moves to the right, the volume of the chamber is reduced and the pressure is increased, the suction valve closes but the discharge valve opens, the working fluid present in the chamber is expelled out of the pump. In this process, the pump is in discharge stroke.

Since the suction stroke and discharge stroke proceed alternatively in a period of time at a constant rotating speed, the pump operational parameters, such as volume flow rate, inlet and outlet pressures and NPSHr are immediate or in pulse. However, their mean values in the period are constant. Based on the pump specification charts, the mean pump flow rate, Q, and NPSHr, are written as

$$\begin{cases} Q = n\left(2.6011 \times 10^{-8}p^2 - 5.6220 \times 10^{-6}p + 1.9298 \times 10^{-3}\right) \\ \text{NPSHr} = 9.2805 \times 10^{-7}n^2 + 9.7480 \times 10^{-5}n + 2.7592 \end{cases} \quad (1)$$

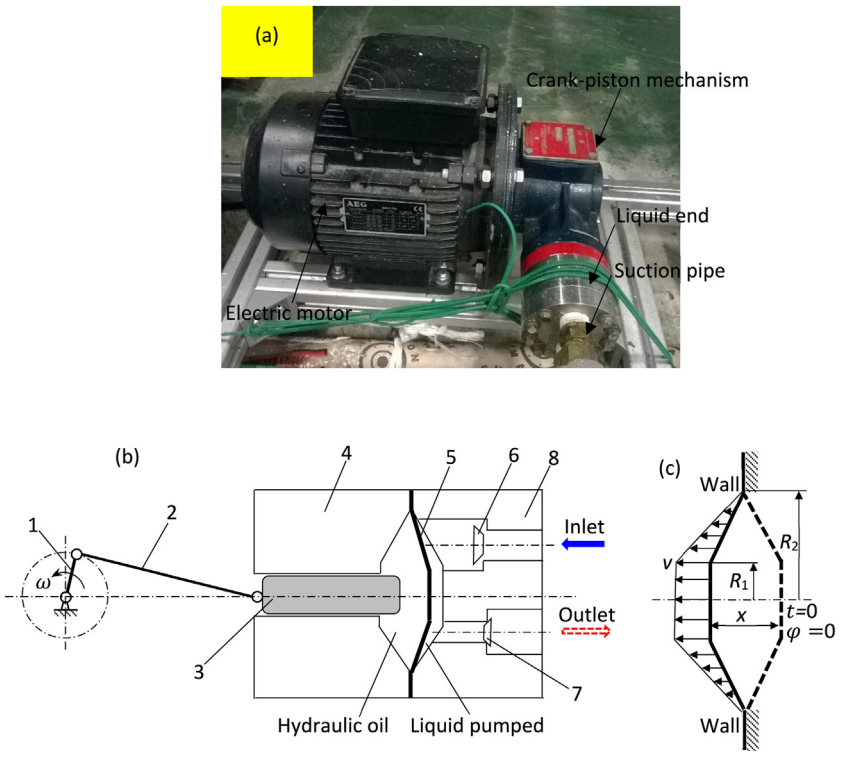

Fig. 1. The picture and sketch of the positive displacement diaphragm pump of G20-E model produced by Wanner Engineering, Inc, 1-drive crank, 2-connecting rod, 3-piston, 4-piston casing, 5-diaphragm, 6-inlet valve, 7-discharge valve, 8-valve housing.

where n is pump rotating speed, rpm, p is pump nominal operational pressure, bar. The Q and NPSHr predicted with the models in Eq. (1) are compared with the data in the pump specification charts in Fig. 2. The two parameters are affected mainly by pump rotating speed. Note that these mean parameters in the pump specification charts were measured by using cold (around 20° room temperature) water. The pump operational pressure in our experiments ($p < 3.5$ bar) has little influence the mean flow rate.

The mean flow rate is related to the flow induced by the periodic motion of the diaphragm in a diaphragm pump. The diaphragm is a flexible rubber material, therefore, fluid–structure interaction analysis or visualization experiments are required to completely understand its motion and deformation characteristics (van Rijswick et al., 2016). Since our aim in the paper is to explore the possibility of cavitation in the suction valve, the actual diaphragm motion is out of the scope of the paper. Here we just use an idealized diaphragm motion and deformation pattern to estimate the periodic flow rate through the suction valve in $s = 4.98$ mm working stroke measured.

The idealized diaphragm motion and deformation is demonstrated in Fig. 1c. In the motion, the diaphragm retains flat cone shape with two radii $R_1 = 5.75$ mm, $R_2 = 15.75$ mm and a variable cone height/displacement x, $x \in [0, s]$. As $x = s/2$, the diaphragm becomes a circular plane. The top surface with the radius $R_1 = 5.75$ mm is in motion with the same speed as the piston, v. The cone surface stroke is assumed to reduce to zero at $R_2 = 15.75$ mm from s at $R_1 = 5.75$ mm linearly. Thus, the stroke profile along the diaphragm is expressed as

$$\begin{cases} s_{top} = s & \text{top plane} \\ s_{cone} = s\left(\dfrac{R_2 - R}{R_2 - R_1}\right) & \text{cone surface} \end{cases} \tag{2}$$

Taking the diaphragm shape in the beginning of suction stroke, i.e. $t = 0$ or $\varphi = \omega t = 0$, as reference configuration, and neglecting the 2nd-order terms (Sahoo, 2006; Lee et al., 2015; Wu et al., 2019), the diaphragm displacement equation is written as

$$x = \begin{cases} 0.5\ s\,(1 - cos\varphi) & \text{top plane} \\ 0.5\ s\left(\dfrac{R_2 - R}{R_2 - R_1}\right)(1 - cos\varphi) & \text{cone surface} \end{cases} \tag{3}$$

The diaphragm moving velocity can be determined by taking the first derivative of x with respect to t, namely

$$v = \frac{dx}{dt} = \frac{dx}{d\varphi}\frac{d\varphi}{dt} = \begin{cases} 0.5\ s\ \omega sin\varphi & \text{top plane} \\ 0.5\ s\ \omega\left(\dfrac{R_2 - R}{R_2 - R_1}\right) sin\varphi & \text{cone surface} \end{cases} \tag{4}$$

Since the suction stroke occurs in $\varphi = [0, \pi]$, there is a flow rate in the suction pipe during this period; otherwise, the flow rate is zero in the pipe. The instantaneous flow rate in the suction pipe during $\varphi = [0, \pi]$ is calculated by

$$q = \int_0^{R_1} s\omega\pi R sin\varphi dR + \int_{R_1}^{R_2} s\omega\pi R\left(\frac{R_2 - R}{R_2 - R_1}\right) sin\varphi\ dR \tag{5}$$

and the equation can be simplified into the following form

$$q = \left(\frac{3R_2^2 + R_1R_2 + R_1^2}{3}\right)\left(\frac{\pi s\omega}{2}\right) sin\varphi = V_s\omega sin\varphi \tag{6}$$

where V_s is the diaphragm stroke volume, $V_s = \pi s\left(3R_2^2 + R_1R_2 + R_1^2\right)/6$. The mean flow rate in the suction pipe in the period of $\varphi = [0, 2\pi]$ should be calculated by

$$Q = \frac{1}{2\pi}\int_0^{\pi} q d\varphi = \left(\frac{3R_2^2 + R_1R_2 + R_1^2}{3}\right)\left(\frac{s\omega}{2}\right) = \frac{V_s\omega}{\pi} \tag{7}$$

If the diaphragm geometrical parameters, R_1 and R_2, piston stroke s and rotational angular speed ω are known, the instantaneous and mean flow rates can be estimated with Eqs. (6) and (7), respectively.

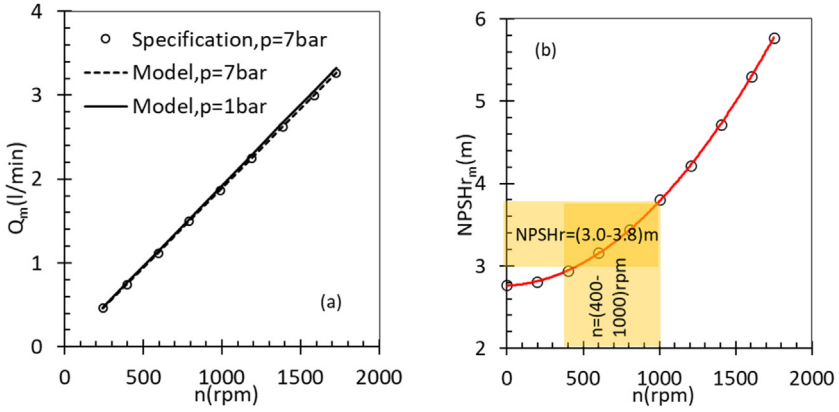

Fig. 2. The predicted mean flow rate and net positive suction head required (NPSHr) as a function of rotational speed, (a) mean flow rate-rotational speed curves, (b) mean NPSHr-rotational speed curve.

2.2. Method for NPSHr correction

Usually, the NPSHr presented in Eq. (1) is measured by using cold water in the pump manufacture's laboratory. This NPSHr is reduced when the pump delivers an organic fluid such as R245fa because of thermodynamic effect in cavitation process. The reduction effect on NPSHr in an ORC system is not commonly known.

The thermodynamic effect in cavitation was introduced in 1945 (Fisher et al., 1945). The thermodynamic effect results in heat transfer between a cavitating spot and its surrounding liquid. During the heat transfer, the surrounding liquid supplies an amount of heat via a heat flux to the cavitating spot to perpetuate the cavitation. The heat flux is driven by the difference in temperature from the surrounding liquid to the spot. This fact suggests the temperature of the surrounding liquid T_l is higher than the temperature in the spot T_v, i.e. there is a temperature depression from the liquid to the cavitating spot, ΔT $(= T_l - T_v)$. Ideally, the pressure in the cavitating spot is equal to the saturated vapour of the liquid at T_v. Clearly, a vapour depression Δp $(=p_v(T_l) - p_v(T_v))$ exists.

There is a link between ΔT and Δp through a known slope of the saturated vapour pressure–liquid temperature curve, i.e. $\Delta p = (dp_v/dT_l)\,\Delta T$. Since it is quite difficult to measure T_v or $p_v(T_v)$, $p_v(T_l)$ has been adopted to calculate NPSHr in experiments for convenience. In reality, NPSHr should be based on $p_v(T_v)$. NPSHr correction means that a correction is applied to a $p_v(T_l)$-based NPSHr to obtain the $p_v(T_v)$-based NPSHr. The key thing in the correction is to find a temperature depression ΔT or pressure depression Δp for a specific liquid pumped in terms of the similarity of cavitation for different liquids, i.e. thermodynamic factor.

Roughly, there are five correction methods for thermodynamic effect in cavitation, namely, B factor, B_1 factor, B_t factor, Σ factor and NPSH formula-based approach. A comprehensive and critical review of these methods is present in Appendix. Σ factor method in Arakeri (1999) is adopted to perform NPSHr correction for the diaphragm pump here. In comparison with the other methods, Σ factor method can decide whether a pump needs cavitation correction or not based on the Σ factor value of the pumped liquid and the pump operating condition. A correlation curve of NPSHr correction can easily be generated in terms of a reduced liquid temperature. This method is straightforward and easily implemented in any applications. In the following, this method is adopted to predict NPSHr when the diaphragm pump delivers the organic fluid-R245fa.

The method relies on a cavitation criterion that is composed of a dimensional thermodynamic parameter Σ and an impeller cavitation performance variable Λ of centrifugal pump such as:

$$\begin{cases} \Sigma = \dfrac{L^2 v_l^2}{T_l c_p v_v^2 \sqrt{\alpha}},\ \Lambda = \left(\dfrac{V_\infty^3 \sigma_l}{D}\right)^{1/2} \\ \Lambda < \Sigma,\ \text{boiling} \\ \Lambda > \Sigma,\ \text{cavitation} \end{cases} \tag{8}$$

In the boiling state, the liquid temperature remains unchanged without thermodynamic effect. In the cavitation state, the thermodynamic effect occurs and the temperature in the cavity is lower than the surrounding liquid during cavitation. According to this fact, a Σ and Λ-based method was developed in Arakeri (1999) to predict NPSHr (T_l) of hot water or hydrocarbons or cryogens. The procedure is as follows:

(1) Determine an appropriate liquid temperature T_l^* with the condition $\Lambda = \Sigma$ for a given pump and liquid pumped with the known V_∞, σ_l and D;

(2) If the pump operating liquid temperature yields $T_l \le T_l^*$, then there is no thermodynamic effect in cavitation, no NPSHr (T_l) correction is applied;

(3) If the temperature is in line with $T_l > T_l^*$, then NPSHr (T_l) correction is required. The NPSHr (T_l) experimental data in Salemann (1959), Stepanoff (1961) and Spraker (1965) was reprocessed by Arakeri (1999) and the correction ΔNPSHr was correlated to the reduced temperature T_R $[=(T_l - T_l^*)/(T_c - T_l^*)]$, T_c is the critical temperature of the liquid. The $\Delta\text{NPSHr} - T_R$ curves and the corresponding scattered experimental data are illustrated in Fig. 3.

The hot water data can be best fitted by a linear model, but those of the other liquids are better represented by a 3rd-order polynomial, the corresponding regression equations are read as

$$\begin{cases} \Delta\text{NPSHr} = 9.8866 T_R - 2.20269,\ R^2 = 0.9583,\ \text{hot water} \\ \Delta\text{NPSHr} = 261.92 T_R^3 - 238.63 T_R^2 + 78.431 T_R - 8.6146, \\ R^2 = 0.973,\ \text{other liquids} \end{cases} \tag{9}$$

where R^2 is R squared goodness of fit. If T_R is known, then the corresponding ΔNPSHr of hot water or other liquids can be estimated with Eq. (9).

ΔNPSHr is the NPSHr correction to a pump at fixed rotative speed and impeller diameter as well as the same working point, meaning $nD/n_{ref}D_{ref} = 1$. Consequently, Eq. (A.35) in Appendix is simplified to the following expression

$$\text{NPSHr}(T_l) + \Delta p_v/\rho_l g = \text{NPSHr}(T_l)_{ref} + (\Delta p_v/\rho_l g)_{ref} \tag{10}$$

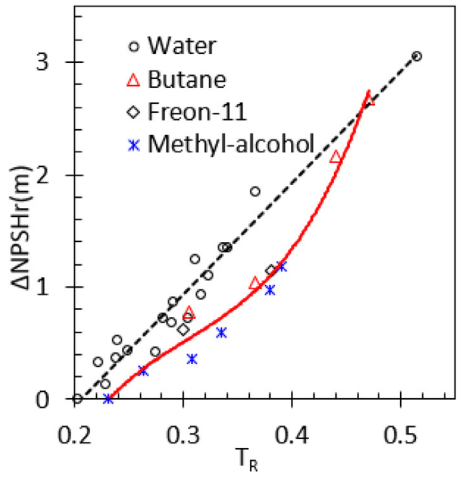

Fig. 3. The correction ΔNPSHr is plotted as a function of the reduced liquid temperature T_R based on the NPSHr experimental data in Salemann (1959), Stepanoff (1961) and Spraker (1965) of water, butane, Freon-11 and methyl-alcohol.

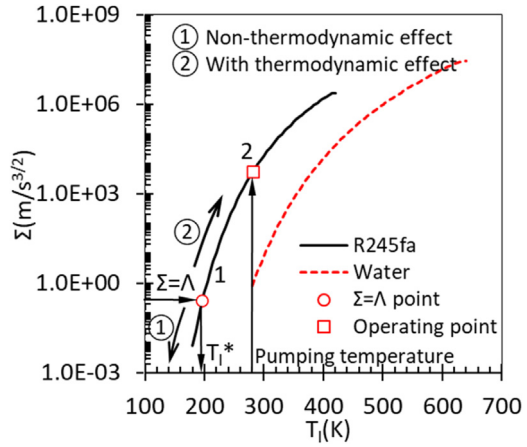

Fig. 4. The thermodynamic parameter Σ of the liquid R245fa is present as a function of the liquid temperature, $T_l^* = 196.27$ K, the pumping temperature $T_l = 281.55$ K, the Σ of water is also shown for comparison.

Noting $\Delta\text{NPSHr} = \Delta p_v/\rho_l g - (\Delta p_v/\rho_l g)_{ref}$, the relationship between NPSHr (T_l) and NPSHr $(T_l)_{ref}$ is given by

$$\text{NPSHr}\,(T_l) = \text{NPSHr}\,(T_l)_{ref} - \Delta\text{NPSHr} \tag{11}$$

If one knows NPSHr $(T_l)_{ref}$ of a liquid at a temperature, then ΔNPSHr of the liquid at another temperature can be calculated, finally one can predict NPSHr (T_l) of that liquid at that temperature. Usually, NPSHr $(T_l)_{ref}$ is for cold water in industry, and ΔNPSHr is for a liquid other than water. Eq. (11) allows one to have NPSHr (T_l) of that liquid.

Since it yields $\Delta\text{NPSHr} \geq 0$, NPSHr (T_l) of that liquid is always smaller than NPSHr $(T_l)_{ref}$ of cold water. Nevertheless, a pump is subject to a lowered NPSHr when pumping hot water, hydrocarbons or cryogens or organic fluid compared with that when handling cold water.

2.3. NPSHr correction implementation and subcooling

The diaphragm pump lifts the organic fluid-R245fa in the experimental loop from $T_l = 8.4$ °C (281.6 K), $p_1 = 1.41$ bar (141 kPa) to $p_2 = 3.73$ bar (373 kPa) at $n = 480$ rpm rotative speed. The characteristic liquid velocity in the suction chamber is $V_\infty = 0.19$ m/s, the characteristic diameter of the chamber is $D = 18$ mm. The head across the pump is $H = (p_2 - p_1)/\rho_l g = 17.1$ m, where $\rho_l = 1382.4$ kg/m^3. According to Eq. (1), NPSHr $(T_l)_{ref}$ is 3.02 m at 480 r/min. The cavitation number is approximately $\sigma_l \approx \text{NPSHr}\,(T_l)_{ref}/H = 0.18$.

The specific heat capacity c_p, thermal diffusivity α, specific volume v_l and latent heat L of the liquid R245fa, vapour pressure p_v, specific volume v_v of the vapour R245fa are best fitted by the following expressions in terms of liquid temperature T_l ranged in 180 K and 420 K

$$\begin{cases} c_p = 2.4T_l + 595.3 \ \text{(J/(kg K))} \\ \alpha = 10^{1.9406\times10^{-12}T_l^5 - 2.6866\times10^{-9}T_l^3 + 1.4736\times10^{-6}T_l^3 - 3.9740\times10^{-4}T_l^2 + 5.2261\times10^{-2}T_l - 9.9567} \\ \quad \times \text{(m}^2\text{/s)} \\ v_l = 10^{2.2308\times10^{-10}T_l^4 - 2.3831\times10^{-7}T_l^3 + 9.5314\times10^{-5}T_l^2 - 1.6119\times10^{-2}T_l - 2.2391} \ \text{(m}^3\text{/kg)} \\ L = -8.7719\times10^{-8}T_l^4 + 9.0425\times10^{-5}T_l^3 - 3.4842\times10^{-2}T_l^2 + 5.3981T_l \\ \quad -2.5688\times10^{1} \ \text{(kJ/kg)} \\ p_v = 10^{3.2105\times10^{-7}T_l^3 - 3.6591\times10^{-4}T_l^2 + 1.4850\times10^{-1}T_l - 1.8065\times10^{1}} \ \text{(kPa)} \\ v_v = 10^{-3.6575\times10^{-7}T_l^3 + 3.9504\times10^{-4}T_l^2 - 1.5303\times10^{-1}T_l + 1.9255\times10^{1}} \ \text{(m}^3\text{/kg)} \end{cases} \tag{12}$$

where the thermal conductivity of the liquid R245fa is a constant of $k = 0.087$ W/(m K) in the α expression. The thermodynamic parameter Σ of the liquid R245fa was calculated with the related parameters represented by Eq. (12) and exhibits the following regression equation

$$\Sigma = 10^{5.9660\times10^{-7}T_l^3 - 6.8003\times10^{-4}T_l^2 + 2.7359\times10^{-1}T_l - 3.2656\times10^{1}} \tag{13}$$

Based on the condition $\Lambda = \Sigma$, the appropriate liquid temperature T_l^* is determined to be $T_l^* = 196.27$ K. Obviously, T_l^* is below the pump operating temperature $T_l = 281.6$ K, shown in Fig. 4 where the Σ of water is illustrated for comparison; consequently, the thermodynamic effect must be taken into account when determining NPSHr (T_l).

Considering the critical temperature of the liquid R245fa $T_c = 427.01$ K, the reduction temperature of the liquid is $T_R = 0.3696$, and the corresponding NPSHr correction $\Delta\text{NPSHr} = 1.00$ m is calculated with the second expression in Eq. (9). Eventually, when the pump transports the liquid R245fa, the corresponding NPSHr should be predicted by the following

$$\text{NPSHr}\,(T_l) = \text{NPSHr}\,(T_l)_{ref} - \Delta\text{NPSHr} = 3.02 - 1.00 = 2.02 \ \text{m} \tag{14}$$

Next, the effect of inlet pressure on the pump cavitation performance will be examined. Considering two inlet pressures $p_1 = 1.0$ bar (100 kPa), 1.41 bar (141 kPa), the NPSHa for these inlet pressures are evaluated with

$$\text{NPSHa}\,(T_l) = \frac{p_1 - p_v\,(T_l)}{\rho_l g} \tag{15}$$

The NPSHa values predicted with the two inlet pressures are tabulated in Table 1. The NPSHa at $p_1 = 100$ kPa is 1.62 m only and smaller than NPSHr $(T_l) = 2.02$ m specified in Eq. (14). This means that the inlet tank is unable to supply significantly high pressure for the diaphragm pump to prevent cavitation in its suction valve chamber. Specially, this NPSHa value does not meet the NPSH criterion for non-cavitation operation used generally in the pump industry, namely (Deniau, 2009)

$$\text{NPSHa}\,(T_l) > \text{NPSHr}\,(T_l) + 0.5 \ \text{m} \tag{16}$$

where 0.5 m is a safety margin. Thus, the pump should suffer from cavitation problem at $p_1 = 100$ kPa. The NPSHa at $p_1 = 141$ kPa is

Table 1
NPSHa, NPSHr and subcooling of the diaphragm pump at two inlet pressures and 8.4 °C pumping temperature for liquid R245fa at 480 rpm rotating speed.

ρ_l (kg/m^3)	p_1 (kPa)	p_v (kPa)	NPSHa (m)	ΔT_a (°C)	NPSHr (T_l) (m)		ΔT_r (°C)	
					A	B	A	B
1382.4	100 141	77.05	1.69 4.72	6.93 19.35	3.02	2.02	12.38	8.28

A—non-thermodynamic effect, B—with thermodynamic effect.

4.76 m and is higher than NPSHr (T_l) with a 2.64 m safety margin. As a result, p_1 =141 kPa is a more suitable inlet pressure for the diaphragm pump to avoid cavitation.

Note that even though the NPSHr is reduced from that of cold water, the vapour pressure of the R245fa is 77.05 kPa at 8.4 °C (281.55 K) operating temperature, and much higher than 2.34 kPa of water at 20 °C temperature. Therefore, the pump inlet pressure for the liquid R245fa should be 77.05−2.34 = 75.71 kPa higher than the inlet pressure for cold water to prevent cavitation occurrence.

For refrigerants, cavitation can be suppressed by subcooling the fluid to bring the refrigerant saturation down (Sanger, 1968). The NPSHa and NPSHr in Table 1 and cavitation safety margins above can be converted into the subcooling available ΔT_a and subcooling required ΔT_r and subcooling safety margin by using the relationship

$$\Delta T_r = (dT_l/dp)\,\rho_l g \mathrm{NPSHr} \tag{17}$$

where dT_l/dp is the R245fa vapour temperature–pressure curve slope at 8.4 °C operating temperature of the pump. If NPSHr in Eq. (17) is replaced with NPSHa and the cavitation safety margin, respectively, then the degree of subcooling can be determined with Eq. (17). The corresponding values of ΔT_a and ΔT_r are listed in Table 1. The 0.5 m and 2.64 m cavitation safety margins are for 2.05 °C and 10.82 °C subcooling, respectively.

3. Preliminary analytical and experimental confirmation

3.1. 1D analysis of suction valve motion

Cavitation can occur in the suction valve of a diaphragm pump if the valve is designed improperly or the inlet pressure is not high enough during operation of the pump. 1D analysis of suction valve motion may be helpful to identify cavitation issue during operation of a diaphragm pump. The suction valve structure of the diaphragm pump is illustrated in Fig. 5a, which includes four elements, i.e. valve seat, valve, spring and retainer, and its mechanical model is present in Fig. 5b.

Initially, the valve is closed, i.e. contacts with the seat due to the force generated by the spring in a pre-compressed length $h_0 = -0.5$ mm. As the diaphragm moves to the left gradually; the volume of the pumping chamber is increased, and the liquid pressure is depressed. The valve will open suddenly, i.e. moves off the seat as soon as the opening force due to the pressure difference across the valve is larger than the resistance generated by the spring. After the valve's opening reaches the maximum, the valve will be pulled back to the seat by the spring force. In this section, this process is simulated with 1D mechanical model to determine pressure drop during the valve opening and assess risk of cavitation.

Since experimental data of valve motion in the diaphragm pump is unavailable to us, two mechanical models have to be adopted to make sure a similar valve motion characteristic achieved with them. The first mechanical model is the 1st-order model in which both the drag force imposed on the valve by the fluid and the valve mass are neglected. The second is the 2nd-order valve motion equation with the two factors involved. In

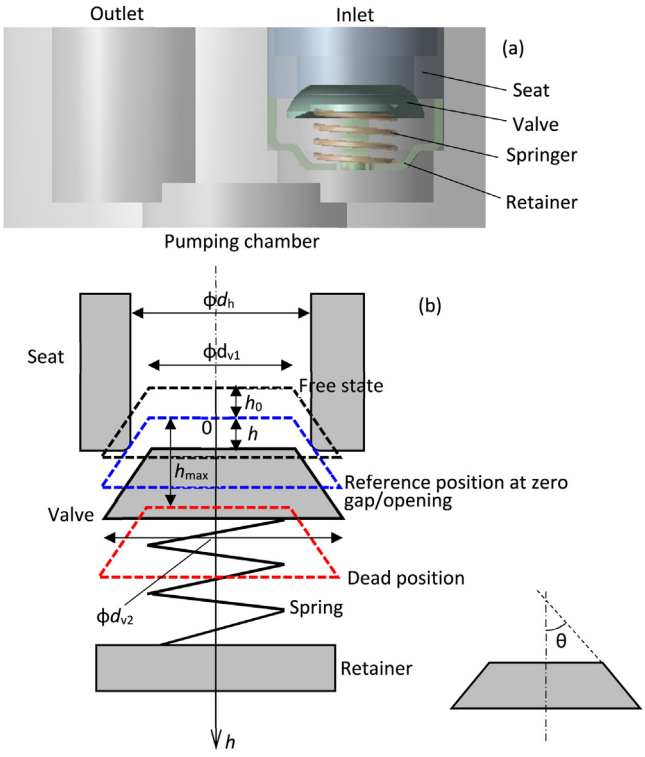

Fig. 5. The suction valve structure (a) and the simplified mechanical model of the valve (b).

both the mechanical models, the fluid is considered incompressible and inviscid, and the fluid flow in front and rear of the valve and through the gap between the valve and the seat is 1D. The historical effects of fluid viscosity are taken into account with flow coefficient through the valve gap and drag coefficient of the valve body.

In the 1st-order mechanical model, the governing equations of valve motion consist of fluid continuity equation and force balance equation of the valve. The continuity equation for incompressible fluids reads as

$$q = q_g + q_v \tag{18}$$

where q is the instantaneous volumetric flow rate in the suction pipe, q_g is the flow rate through the gap between the valve and the seat, and q_v is the flow rate along with the moving valve. q_g and q_v are expressed as

$$q_g = C_q \pi d_h h \sin\theta \sqrt{2\Delta p/\rho_l},\ q_v = \left(\pi d_{v1}^2/4\right)\omega dh/d\varphi \tag{19}$$

where C_q is the flow coefficient through the gap, d_h is the seat diameter, d_h = 18 mm, h is the valve lift, θ is the half of cone apex angle, Δp is the pressure difference across the valve, ρ_l is the density of the liquid pumped, d_{v1} is the diameter of the upper base of the valve, d_{v1} = 14 mm, $v = \omega dh/d\varphi$ is valve moving velocity, where ω is the angular speed of diaphragm reciprocating motion, $\omega = \pi n/30$, n is the rotational speed of the pump driver.

The force balance equation of the valve is the application of Newton's second law of motion to the valve. When the valve mass and drag force are ignored and the equation is written as

$$0 = \Delta p \frac{\pi}{4} d_h^2 - k\,(h + h_0) \tag{20}$$

where k is the spring stiffness.

Substitute Eqs. (6), (18) and (19) into Eq. (20), the governing equation of the valve motion is obtained

$$\frac{\pi d_{v1}^2}{4}\omega\frac{dh}{d\varphi} + C_q \pi d_h h sin\theta \sqrt{\frac{2k\,(h + h_0)}{\frac{\pi d_h^2}{4}\rho_l}} - V_s \omega sin\varphi = 0 \tag{21}$$

Eq. (20) is a 1st-order ordinary differential equation and can be solved for valve lift h numerically by using the 4th-order Runge–Kutta method (Griffiths and Smith, 1991) with the following initial condition

$$h|_{\varphi=0} = 0 \tag{22}$$

The valve is subject to a pressure reduction in the gap at $\varphi = 0$ as the diaphragm starts to move. The pressure reduction can be obtained from Eqs. (20) and (22) as follows

$$\Delta p|_{\varphi=0} = (kh_0)\left(\frac{4}{\pi d_h^2}\right) \tag{23}$$

In Eq. (21), the flow/discharge coefficient C_q through the gap between the valve and the seat is the key factor determining the valve opening. There is no such a flow coefficient measured on an actual valve in diaphragm pumps presently. Thus, based on the empirical correlation of hydraulic loss coefficient ξ for conical/poppet valves (Idelchik, 1966), the correlation of C_q has to be proposed by employing the relationship $C_q = 1/\sqrt{\xi}$, as such

$$C_q = 71.374(h/d_h)^4 - 100.29(h/d_h)^3 + 30.349(h/d_h)^2 + 0.0849(h/d_h) + 0.1284 \tag{24}$$

Finally, Eqs. (21), (22) and (24) form a 1st-order mechanical model for clarifying characteristics of the valve motion in the diaphragm pump.

If the valve mass and fluid drag force are considered, the force balance equation of the valve is expressed as

$$m_v \omega^2 \frac{d^2 h}{d\varphi^2} = \Delta p \frac{\pi}{4} d_h^2 - F_R - k\,(h + h_0) \tag{25}$$

where m_v is the mass of the valve, F_R is the drag force imposed by the pumped liquid, the drag force is related to the draft coefficient, C_D, and the squared velocity difference between the flow in the gap and the valve itself, as well as the projection area of the valve, i.e.

$$F_R = C_D \frac{\rho_l \left(v_g - v\right)^2}{2}\frac{\pi d_{v2}^2}{4},\ v_g = \frac{q_g}{\pi d_h h \sin\theta},\ v = \omega\frac{dh}{d\varphi} \tag{26}$$

where v_g is the velocity of the pumped liquid through the gap, v is the valve velocity, d_{v2} is the lower base diameter of the valve, d_{v2} = 21 mm, the drag coefficient $C_D = 0.65$ is after (White, 2011).

Combining Eqs. (18) and (19), (25) and (26), respectively, the governing equations for the valve motion are in the following forms

$$\begin{cases} \left(\pi d_{v1}^2/4\right)\omega\dfrac{dh}{d\varphi} = V_s\omega\sin\varphi - C_q\pi d_h h\sin\theta\sqrt{2\Delta p/\rho_l} \\ m_v\omega^2\dfrac{d^2h}{d\varphi^2} = \Delta p\dfrac{\pi}{4}d_h^2 - C_D\dfrac{\rho_l\left(v_g - v\right)^2}{2}\dfrac{\pi d_{v2}^2}{4} - k\,(h + h_0) \end{cases} \tag{27}$$

To facilitate implementing the 4th-order Runge–Kutta method, Eq. (27) is decomposed into a set of three 1st-order ordinary differential equations

$$\begin{cases} \dfrac{dh}{d\varphi} = \omega h_1 \\ \left(\pi d_{v1}^2/4\right)\omega h_1 = V_s\omega\sin\varphi - C_q\pi d_h h\sin\theta\sqrt{2\Delta p/\rho_l} \\ m_v\omega^2\dfrac{dh_1}{d\varphi} = \Delta p\dfrac{\pi}{4}d_h^2 - C_D\dfrac{\rho_l\left(v_g - v\right)^2}{2}\dfrac{\pi d_{v2}^2}{4} - k\,(h + h_0) \end{cases} \tag{28}$$

To guarantee the solution of Eq. (28), the following initial conditions are needed

$$\begin{cases} h|_{\varphi=0} = 0 \\ h_1|_{\varphi=0} = 0 \end{cases} \tag{29}$$

Furthermore, the valve is subject to a pressure reduction in the gap at $\varphi = 0$ as the diaphragm starts to move with the maximum acceleration. Taking the derivative of the second expression in Eq. (28), we have

$$\frac{dh_1}{d\varphi} = V_s\cos\varphi\left(\frac{4}{\pi d_{v1}^2}\right) \tag{30}$$

Because of $F_R = 0$ and $h = 0$ at $\varphi = 0$, Combining Eq. (29) and the last expression in Eq. (28) results in the pressure reduction

$$\Delta p|_{\varphi=0} = \left(kh_0 + m_v\omega^2\left.\frac{dh_1}{d\varphi}\right|_{\varphi=0}\right)\left(\frac{4}{\pi d_h^2}\right) \tag{31}$$

After the governing equations for the valve motion Eq. (21) or (27) are solved, the pressure drop across the gap is available. The pressure at the gap outlet can be calculated at a known pump inlet pressure p_1, and the expression is written as

$$p = p_1 - \Delta p \tag{32}$$

The equations above were coded in MATLAB 2018b. To obtain accurate solutions, the suction stroke $\varphi = \pi(180°)$ is divided into 300 elements, and the governing equations are integrated over the elements by using the 4th-order Runge–Kutta method. The input data to the code is listed in Table 2 and the corresponding results are illustrated in Fig. 6.

In the figure, the results predicted with the 2nd-order mechanical model such as valve lift, velocity, force and pressures, exhibit a slightly pulsatile behaviour in high frequency during the opening process. The valve shows more delay in the valve lift and velocity during the opening and closing processes based on the 1st-order model than the 2nd-order model. However, the highest valve lift is very similar in both the models. The drag force is

Table 2
The parameters of the diaphragm pump and liquid pumped in 1D simulations.

Item	Parameter	Numerical figure
Liquid pumped at 8.4 °C (281.55 K)	ρ (kg/m^3)	1382.4
	μ (Pa s)	5.0570 $\times 10^{-4}$
	p_v (kPa)	77.05
Diaphragm	R_1 (mm)	5.75
	R_2 (mm)	15.75
	s (mm)	4.938
	n (rpm)	480
	ω (rad/s)	150.80
Valve	m_v (kg)	0.0825
	d_h (mm)	14
	d_{v1} (mm)	18
	d_{v2} (mm)	21
	θ(°)	45
Spring	k (N/m)	900
	h_0 (mm)	−0.5
Operating condition	p_1 (kPa)	100
		141

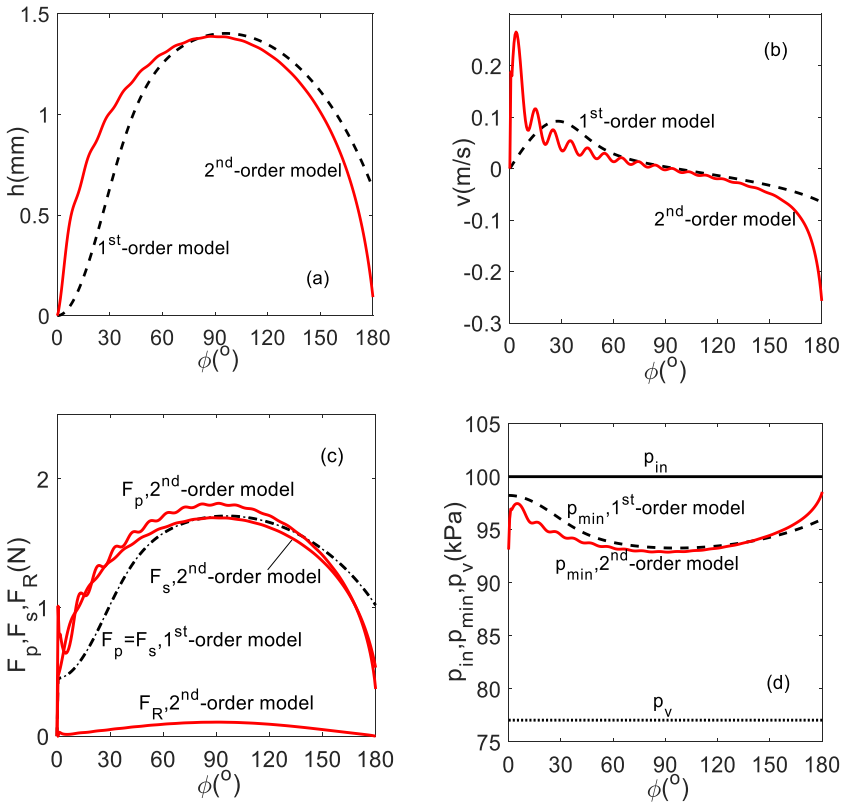

Fig. 6. The valve opening h (a), velocity v (b), force due to pressure difference F_p, spring force F_s, fluid drag force F_R (c), minimum pressure at the gap outlet p (d) predicted with the 1st-order and 2nd-order mechanical models.

minor in comparison with the spring force and the force induced caused by the pressure difference across the valve.

The minimum pressure at the outlet of the gap predicted by the 2nd-order model at $\varphi = 0°$ is the lowest, but still higher than the liquid–vapour pressure, suggesting cavitation may not occur. The minimum pressure predicted by the 1st-order mechanical model is always higher than the pressure predicted by the 2nd-order mechanical model at $\varphi \leq 130°$.

The fluid pressure at the gap outlet depends on flow rate (phase angle of the diaphragm). For the 2nd-order mechanical model, the fluid pressure is the lowest at $\varphi = 0°$ imposed by the initial condition Eq. (30). As $\varphi > 0°$ the pressure rises sharply, and then declines slowly until the maximum flow rate, and finally rises steadily. This trend suggests cavitation can occur at the beginning of the suction stoke and the maximum flow rate in the diaphragm pump. For the 1st-order mechanical model, the lowest pressure is predicted at the maximum flow rate only.

Based on the results, it is understood that even though the valve motion characteristics can be captured by using the 1st- and 2nd-order mechanical models, the pressure drop across the gap is predicted by using the empirical flow coefficient. The local minimum fluid pressure in the gap, which is responsible for cavitation inception and development, cannot be captured, because the flow details through the gap cannot be resolved with the very simple 1D flow model. Nevertheless, CFD simulation in the pump suction chamber must be carried out when the diaphragm pump is handling liquid R245fa.

3.2. Preliminary experiment

A test rig, which is demonstrated in Fig. 7, was built to clarify the cavitation performance of a diaphragm pump in an ORC system. The rig is composed of the evaporator, expander, condenser and diaphragm pump. The liquid receiver accommodates the liquid R245fa discharged from the condenser and feeds it to the pump. The DaqVIEW was used to acquire experimental data from the temperature and pressure and flow rate sensors.

The expander (Air Squared: E15H022A-SH) works at 70 °C inlet temperature and 4 bar inlet pressure, 50 °C outlet temperature and 1 bar outlet pressure at 0.022 kg/s mass flow. The expander is directly coupled to a single-phase generator (Voltmaster: AB30L WEIPU) with any generated power being dissipated by three 400 W lamps.

The heating loop produces 93 °C water for the evaporator at 7 l/min flow rate, the cold loop temperature has a 3 °C variation between 7 °C and 10 °C with a cooling flow rate of 10 l/min.

The diaphragm pump (Hydra-cell G20 EDSPHFEHG) was connected to a three phase 6 pole motor (AEG: AM 80z AA 6). A frequency inverted was used to vary the pump supply frequency (AEG: AM 80z AA 6).

The monitored pressure and temperature time-history curves are illustrated in Fig. 8 at the pump inlet and outlet when the pump is running at 480 rpm under 1.41 bar mean inlet pressure condition. The pump outlet pressure seems noisy, and the inlet pressure, inlet and outlet temperature profiles exhibit a periodic oscillation (the periodicity $\approx$ 10 min). In Section 2.3, the 1.41 bar mean inlet pressure corresponds to a safety margin as high as 2.64 m, thus the oscillation is unlikely attributed to cavitation in the suction chamber.

The monitored temperature time-history curves at the inlet and outlet of the evaporator and condenser are plotted in Fig. 9a and b, and the pressure and temperature profiles at the inlet and outlet of the expander are also involved for an additional examination. Clearly, it is only the temperature profile at the condenser inlet that can exactly match the temperature profiles at the pump

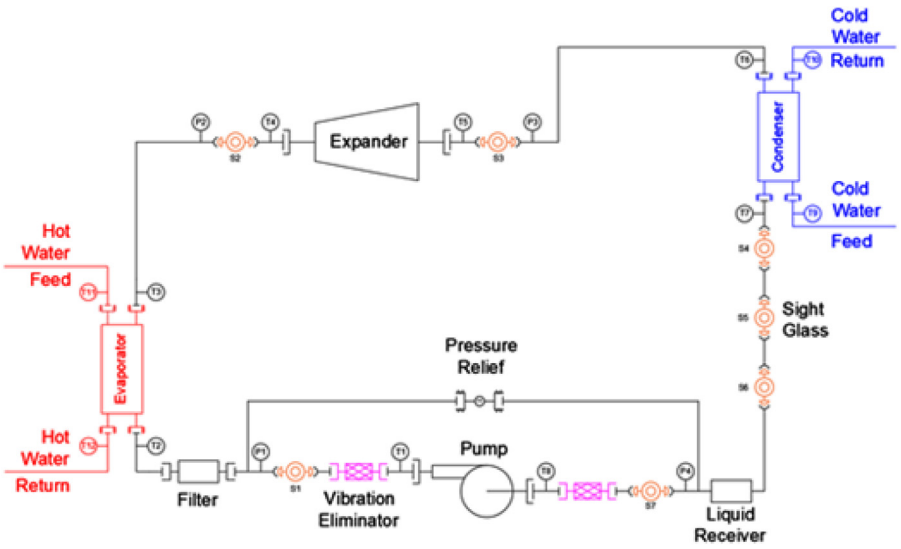

Fig. 7. The test rig flow chart of an organic Rankine cycle system to investigate cavitation performance of the diaphragm pump.

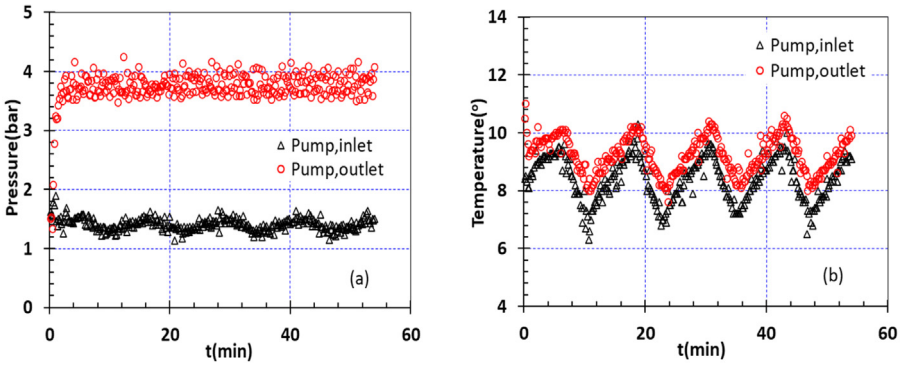

Fig. 8. The monitored pressure and temperature at the pump inlet and outlet, 480 rpm rotational speed.

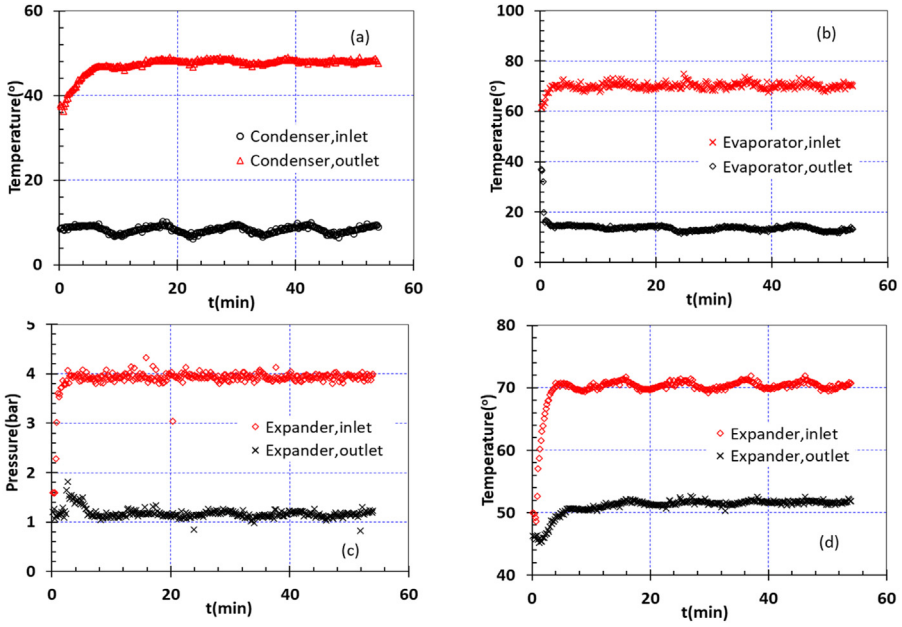

Fig. 9. The monitored temperature at the inlet and outlet of the condenser, evaporator and expander as well as the pressure at the inlet and outlet of the expander.

inlet and outlet and the pressure profile at the pump inlet, respectively. Nevertheless, the temperature profile at the condenser inlet should be responsible for the pressure and temperature oscillation at the pump inlet and the temperature fluctuation

at the pump outlet. Further work, including condenser inflow condition inspection and the pump performance measurements under various mean inlet pressures should be conducted.

3.3. Discussion

The performance of a specific diaphragm pump which is potentially applied to ORC systems was estimated based on the existing performance charts produced by the manufacture in terms of pump rotating speed and inlet liquid pressure when pumping cold water. In the article, the cavitation performance of a specific diaphragm pump was estimated by considering thermodynamic effect in cavitation of organic liquid R245fa based on the existing NPSHr correction method for centrifugal pumps but with a regression equation fitted. Such an analytical estimation for diaphragm pumps has not appeared in the literature so far. The study presented here can be meaningful in the selection of diaphragm pumps for ORC systems.

The subcooling estimated for the diaphragm pump-Hydra-Cell G20-E model is 8.28 °C and 12.38 °C respectively with and without the thermodynamic effect, as listed in Table 1. There is not directly experimental evidence to support these predictions presently. Fortunately, two experimental observations may be favourable to the estimations. For example, when pumping organic liquid R245fa, for a reciprocating plunger pump, the subcooling is 13 °C (Chang et al., 2015). For liquid R134a, the tested subcooling of the diaphragm pump-Hydra-Cell G03X model was 4.4 °C (Landelle et al., 2015, 2017).

In practice, except increasing organic fluid container pressure and subcooling, as common measures, a booter pump is often installed in front of the diaphragm pump to raise the inlet pressure of the pump to prevent cavitation.

The cavitation in positive displacement reciprocating pumps is related to liquid acceleration head and water hammer effect in the suction pipeline or the interaction between naturally pulsating reciprocating pumps and the piping system (Sahoo, 2006; Parry, 1986; Vetter and Schweinfuter, 1987; Wachel et al., 1989; Singh and Able, 1996). Whether the piping system is concerned in the cavitation depends on pump power density index (PDI) (Singh and Able, 1996)

$$PDI = 2 \times 10^{-6} \times n \times s \times H \tag{33}$$

where n is strokes per minute per liquid chamber, s is stroke in inches, H is pump head rise in ft. If PDI is less than 0.02, piping system has negligible effect on the cavitation in the pump, so the liquid acceleration head and water hammer effect in the suction pipeline can be ignored (Singh and Able, 1996). For the diaphragm pump studied here, its PDI is 0.01, therefore the suction pipeline can be neglected in the mechanical model in Section 3.1.

In Fig. 6a, the valve lift does not become zero when the suction stroke terminates ($\varphi = 180°$). This suggests there is a time lag in the suction valve closing. The models do exactly capture the lag effect.

High-speed camera-based flow visualization observations illustrated that cavitation occurs at the beginning of suction stroke owing to the sudden expansion of suction chamber, but it disappears after the chamber is filled with the liquid and its vapour bubbles collapse off the valve surface. This cavitation is an intrinsic property of reciprocating pumps and harmless to the valve function and pump performance (Opitz and Schlücker, 2010; Opitz et al., 2011). As the suction head is declined, the other cavitation can appear at the maximum flow rate and the vapour bubbles collapse at a low flow rate. This sort of cavitation is flow induced cavitation and can impair the valve function and pump performance, and it must be avoided in reciprocating pump operations (Opitz et al., 2011).

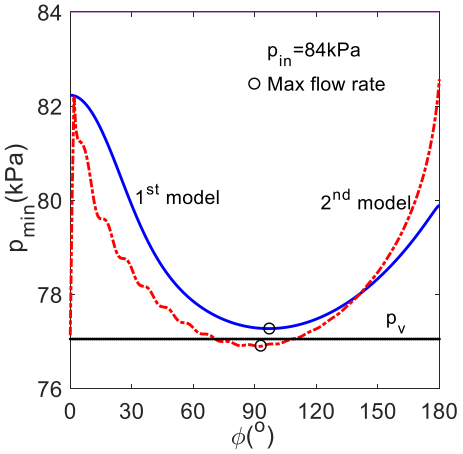

Fig. 10. The pressure profiles at the outlet of valve predicted by using the 1st- and 2nd-order mechanical models at the inlet pressure of $p_{in} = 84$ kPa.

Fig. 10 illustrates the pressure profiles at the gap outlet of valve calculated by the 1st- and 2nd-order mechanical models in suction stroke at the inlet pressure of $p_{in} = 84$ kPa. For the 1st-order mechanical model, the pressure profile has the minimum at the maximum flow rate only, suggesting the flow induced cavitation there. For the 2nd-order mechanical model, however, the pressure profile is with two minimum pressures each at the beginning of suction stroke and at the maximum flow rate, indicating the cavitation due to expansion and flow induced cavitation in the stroke. This outcome seems in agreement with observations made in Opitz et al. (2011). In this context, the 2nd-order mechanical model is more significant than the 1st-order mechanical model. Note that the minimum pressure values may be overpredicted because the model is simple 1D. Nevertheless, 3D cavitating flow simulations in the suction chamber of the diaphragm pump are on demand to capture fluid flow details.

The flow coefficient through the gap between the valve and the vale seat is important to the mechanical models in Section 3.1. There is another flow coefficient based on the flow resistance factor ξ present in Vetter et al. (1989)

$$\begin{cases} \xi = \left(\dfrac{107}{Re} + 1.4\right)\left[74\left(\dfrac{d_h}{h}\right)^{-2.4} + 1\right] \\ C_q = \xi^{-0.5},\ Re = \left(\dfrac{q_g}{\pi d_h h sin\theta}\right)\left(\dfrac{2hsin\theta}{\nu}\right) \end{cases} \tag{34}$$

where Re is Reynolds number of the gap, ν is liquid kinematic viscosity. Based on the 1st-order mechanical model, a comparison of the flow rate coefficients in Eqs. (24) and (34) is illustrated in Fig. 11. Clearly, the value predicted with the correlation of Eq. (34) seems to be too small.

Honestly, the paper suffers from a few limitations. The compressibility of the liquid pumped is not considered. As a result, the diaphragm membrane can instantly respond to the motor rotation without dead angle. The discharge stroke is not involved in the paper, thus the time lag in the discharge valve closing, which can delay the suction valve to open, is not taken into account.

For the analytically approximate instantaneous and mean flow rate formulas, an idealized deformation and shape was assumed in the diaphragm in Section 2.1. Actually, the diaphragm likely experiences a complicated deformation pattern (Vetter et al., 1995) and local buckling (van Rijswick et al., 2016; Vetter et al., 1995). Additionally, the diaphragm was hydraulically driven, as show Fig. 1b. And an underlying assumption that the hydraulic oil

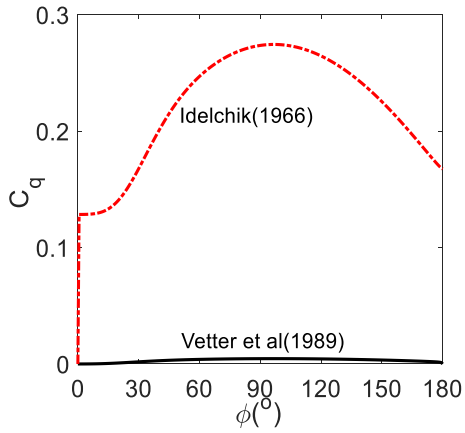

Fig. 11. The flow coefficients determined by two empirical correlations based on Idelchik (1966) and Vetter et al. (1989), respectively.

movement is the same as the piston without any oil leakage was held when the flow rate formulas were deduced. Nevertheless, the instantaneous and mean flow rate formulas provided in the paper need to be corrected by using experimental data in future.

The NPSHr predicted with thermodynamic effect in cavitation has not been validated with experimental observations. Hopefully, the validation will be available in near future.

The experimental data that are used to correct NPSHr are essentially measured from a variety of centrifugal pumps rather than from reciprocating pumps. Naturally, whether those data are applicable to reciprocating pumps is questionable and needs more experimental validations in future.

4. Conclusion

In the article, particular attention was devoted to NPSHr prediction by considering thermodynamic effect in cavitation when the pump feeds the organic liquid R245fa to the evaporator in an ORC system. A comprehensive and critical review was conducted on the thermodynamic effect and the corresponding correction methods for NPSHr of centrifugal pumps. Then the method in Arakeri (1999) was selected and updated to correct the NPSHr of cold water at 480 rpm pump rotational speed to obtain the NPSHr of the liquid R245fa. The 1st- and 2nd-order 1D mechanical models for motion of the suction valve were deduced and solved at 480 rpm and 100 kPa and 141 kPa inlet pressures to characterize the cavitation behaviour of the valve. A preliminary experiment was carried out to confirm the analysed results. The conclusions made include:

(1) When the diaphragm pump delivers the 8.4 °C liquid R245fa at 480 rpm, its NPSHr is reduced to 2.02 m from 3.02 m NPSHr of cold water due to the thermodynamic effect in cavitation, and the corresponding subcooling is reduced to 8.28 °C from 12.38 °C. 100 kPa inlet pressure can lead to cavitation in the pump valve but 141 kPa cannot.

(2) The valve lift, velocity, force and pressures predicted with the 2nd-order mechanical model demonstrate a slightly pulsation in the opening process, while the in the valve lift and velocity based on the 1st-order model exhibit a more delay in the opening and closing processes.

(3) The highest valve lift is very close in both the 1st- and 2nd-order mechanical models; the drag force is minor in comparison with the spring force and the force caused by the pressure difference across the valve.

(4) The pressure profile at the outlet of the valve gap predicted by the 2nd-order mechanical model is with two minimums each at the beginning of suction stroke and at the maximum flow rate, showing the cavitation owing to the initial expansion and the latter cavitation induced by increasing flow rate in the stroke observed (Opitz et al., 2011). The 1st-order mechanical model, however, can capture the minimum pressure at the maximum flow rate only.

(5) The minimum pressure estimation in the 1st- and 2nd-order mechanical models relies completely on the very limited flow coefficients found in the literature, thus the minimum pressure values are inaccurate or overpredicted; consequently, both the models cannot predict the valve cavitation behaviour exactly.

Nevertheless, 3D cavitating flow simulations of organic fluids in the suction chamber of the diaphragm pump are desirable to accurately clarify the valve cavitation performance and capture the corresponding flow details in future.

CRediT authorship contribution statement

Wenguang Li: Investigation, Methodology, Formal analysis, Visualization, Writing - original draft. **Andrew Mckeown:** Investigation-experimental reserch, Writing-review & editing. **Zhibin Yu:** Funding acquisition, Project administration, Writing-review & editing.

Declaration of competing interest

The authors declare that they have no known competing financial interests or personal relationships that could have appeared to influence the work reported in this paper.

Acknowledgements

The work was supported by EPSRC in the UK in terms of grants such as EP/N020472/1, EP/N005228/1, EP/P028829/1 and EP/R003122/1, the support was acknowledged indeed.

Appendix. Review of NPSHr correction methods for thermodynamic effect in cavitation

A.1. Thermodynamic effect

The thermodynamic effect came into a subject in 1945's (Fisher et al., 1945). In that pioneer work, the vapour pressure–temperature relationship of a liquid yields an exponential function, there is a thermal equilibrium between liquid and vapour under adiabatic conditions during cavitation, and the vapour is considered idealized gas, i.e.

$$\begin{cases} p_v = e^{a-b/T_l} \\ W_l c_p \Delta T = L W_v \\ p_v = \dfrac{W_v}{V_v}\dfrac{RT_l}{M} = \rho_v \dfrac{RT_l}{M} = \dfrac{1}{v_v}\dfrac{RT_l}{M} \end{cases} \tag{A.1}$$

where a and b are the constants for the vapour pressure–temperature relationship, p_v is the saturated vapour of liquid, c_p is the specific heat capacity of liquid, L is the latent heat of liquid, M is the molar mass of the vapour, R is the universal gas constant, $R = 8.3145$ J/mol K, T_l is the liquid temperature pumped, W_l is liquid mass considered, W_v is the vapour mass, v_l and v_v are the specific volume of the liquid and vapour, respectively, $v_l = 1/\rho_l$ and $v_v = 1/\rho_v$, ρ_l and ρ_v are the density of the liquid and vapour, $\Delta T(=T_l - T_v)$ is temperature depression in a cavity compared with the temperature of the liquid around the cavity, and $\Delta p_v[=p_v(T_l) - p_v(T_v)]$ is vapour depressions in a cavity compared with the temperature of the liquid around the cavity, T_v is the vapour temperature.

Since $W_l = V_l\rho_l = V_l/v_l$ and $W_v = V_v\rho_v = V_v/v_v$, V_l and V_v are the liquid and vapour volumes, then, the ratio of the specific volume of liquid–vapour mixture v_{vl} to the specific volume of liquid v_l is expressed as

$$\frac{v_{vl}}{v_l} = 1 + \left(\frac{R}{M}\right)\left(\frac{1}{b}\right)\left(\frac{c_p T_l^3}{v_l^2 p_v^2 L}\right)(\Delta p_v v_l) \tag{A.2}$$

where v_{vl} is the specific volume of the vapour–liquid mixture, defined with $v_{vl} = (v_l W_l + v_v W_v)/W_l$.

The parameter $\Delta p_v v_l$ is the loss of head owing to restriction of flow-through cross-section imposed by the cavity. The ratio v_{vl}/v_l was used to characterize the extent of cavitation or the similarity of cavitation. When a pump delivers different liquids at the same temperature, $\Delta p_v v_l$ should be in the following form for the same v_{vl}/v_l

$$\Delta p_v v_l \propto \frac{MLbp_v^2 v_l^2}{c_p} \tag{A.3}$$

This is the first correlation of vapour pressure depression in terms of thermodynamics in cavitation. The pressure depression $\Delta p_v v_l$ is determined mainly by latent heat, specific heat and slope of the $p_v - T_l$ curve of the liquid pumped.

A.2. B, B_1 and B_t factors and their correlations

In Stahl and Stepanoff (1956), the heat balance expression in Eq. (A.1) was adopted to develop the criterion for thermodynamics in cavitation. Considering $W_l = V_l/v_l$ and $W_v = V_v/v_v$, then the heat balance equation is rewritten as

$$B = \frac{V_v}{V_l} = \left(\frac{v_v}{v_l}\right)\left(\frac{c_p \Delta T}{L}\right) = \left(\frac{v_v}{v_l}\right)\left(\frac{c_p \Delta p_v}{L}\right)\left(\frac{dp_v}{dT_l}\right)^{-1} \tag{A.4}$$

where $B = V_v/V_l$ is the ratio of the vapour volume to the liquid volume, called the criterion B or B factor for thermodynamics in cavitation (Stahl and Stepanoff, 1956). B depends on thermodynamic properties (v_v, v_l, c_p, L, dp_v/dT_l) and temperature depression ΔT. In order to calculate the criterion B of various liquids pumped at a temperature T_l, a 1.6 in (0.4 m) vapour pressure depression Δp_v, which means a depression in NPSHr, was given, and the corresponding temperature depression ΔT with a known $p_v - T_l$ relationship, was estimated with $\Delta T = \Delta p_v/(dp_v/dT_l)$. A series of cavitation experiments was conducted on a centrifugal pump with 38 mm suction nozzle diameter at 3470 rpm rotational speed and 1.22 m NPSHa when pumping water at temperatures 21, 82, 100, 121, 149 °C, respectively. B factor values at these temperatures were calculated and discussed (Stahl and Stepanoff, 1956).

NPSHr at 3% head drop was measured in two centrifugal pumps ($N_s = 1200$, 1600, $n = 3585$ rpm) handling water, butane, benzene +3% propane by weight, kerosene degasified, gasoline, and Freon 11 at various temperatures (Salemann, 1959). N_s is specific speed of centrifugal pumps, $N_s = n\sqrt{Q}/H^{0.75}$, Q is pump volume flow rate in US gallon/min, and H is pump head in ft. The NPSHr correction curves were generated for paraffin hydrocarbons and water in terms of vapour pressure and temperature. The NPSHr correction ΔNPSH is defined as the difference in NPSHr of a liquid at a pumping temperature from that of cold water (22 °C) $\mathrm{NPSHr_w}$, namely

$$\Delta\mathrm{NPSH} = \mathrm{NPSHr} - \mathrm{NPSHr_w} \tag{A.5}$$

In Stepanoff (1961), an empirical method was delivered for a liquid pumped at a known pumping temperature based on the criterion B by using two correlations, one is the $B - p_v$ curves at four suction specific speeds such as 6000, 7200, 9000 and 12 000 to cover the experimental data in Salemann (1959), one is Eq. (A.4). The procedure for determining ΔNPSH is rather straightforward, that is $T_l \rightarrow p_v \rightarrow B \rightarrow \Delta T \rightarrow \Delta p_v \rightarrow \Delta$NPSHr, where $\Delta\mathrm{NPSHr} = \Delta p_v/g\rho_l = \Delta T\ dp_v/dT_l/g\rho_l$, g is the acceleration due to the gravity.

Later, that method was updated in Stepanoff (1964) by using the Clausius–Clapeyron equation to estimate dp_v/dT and by establishing analytical relation of ΔNPSHr with both p_v and B_1 which the criterion B at $\Delta\mathrm{NPSHr_1} = 1$ ft. the Clausius–Clapeyron equation reads as (Stepanoff, 1964)

$$\frac{dp_v}{dT} = \frac{L}{T_l(v_v - v_l)} \approx \frac{L}{T_l v_v} \tag{A.6}$$

Substituting Eq. (A.6) for dp_v/dT_l in Eq. (A.4), the criterion B is rewritten as

$$B = \left(\frac{v_v}{v_l}\right)^2\left(\frac{c_p T_l}{L^2}\right)(\Delta p_v v_l) \tag{A.7}$$

Under $\Delta p_{v1} v_l/g = \Delta\mathrm{NPSHr_1}$ condition, the criterion B becomes a specific numerical value denoted by B_1

$$B_1 = \left(\frac{v_v}{v_l}\right)^2\left(\frac{c_p T_l}{L^2}\right)(g\Delta\mathrm{NPSHr_1}) \tag{A.8}$$

It was found that the parameter $B_1\Delta\mathrm{NPSHr}^{3/4}$ can be correlated with $(p_v v_l/g)^{-3/4}$ in a linear relation for the experimental data in Salemann (1959). If the unit of ΔNPSHr and $p_v v_l/g$ is in ft, then the correlation is expressed with

$$B_1\Delta\mathrm{NPSHr}^{3/4} = \frac{22.5}{(p_v v_l/g)^{3/4}} \tag{A.9}$$

In that case, the suction specific speed was excluded from the correlation and ΔNPSHr can be estimated very simply from Eq. (A.9) with known T, v_v, v_l, c_p, L and B_1.

In parallel, the thermodynamic criteria of cavitation were derived based on one-dimensional governing equations of inviscid fluid, including continuity, momentum and energy equations under cavitation and adiabatic conditions (Spraker, 1965) to obtain a general thermodynamic criterion. These equations are written as follows

$$\begin{cases} d(\rho_m u_m) = 0 \\ dp_v + d\left(\rho_m u_m^2\right) = 0 \\ d\psi + d\left(u_m^2/2\right) = 0 \end{cases} \tag{A.10}$$

where ρ_m is the density of a liquid–vapour mixture, $\rho_m = [(1-y)v_l + v_v]^{-1}$, y is the mass percentage of vapour, $y = W_v/(W_l + W_v)$, u_m is the velocity of the mixture, ψ is enthalpy of the mixture, $\psi = \psi_l + yL$, $d\psi_l \approx c_p(dp_v/dT_l)^{-1}dp_v$. Eliminating u_m from Eq. (A.10), dp_v is expressed with v_l, v_v, L, y and dp_v/dT_l

$$dp_v = \frac{Ldy}{(1-y)v_l + yv_v - c_p(dp_v/dT_l)^{-1}} \tag{A.11}$$

Considering that v_l, v_v, L and dp_v/dT_l are constant, Eq. (A.10) is integrated from $y = 0$ to y to estimate pressure depression Δp_v

$$\Delta p_v = \left(\frac{L}{v_v - v_l}\right) ln \frac{1}{1 - \frac{(v_v - v_l)y}{c_p(dp_v/dT_l)^{-1} - v_l}} \tag{A.12}$$

Noting $B = V_v/V_l = W_v v_v/W_l v_l$, then we have

$$y = \frac{V_v/v_v}{V_v/v_v + V_l/v_l} = \frac{B/v_v}{B/v_v + 1/v_l} \tag{A.13}$$

Substituting Eq. (A.13) into Eq. (A.12) for y, a complex analytical relationship between Δp_v and B is resulted

$$\Delta p_v = \left(\frac{L}{v_v - v_l}\right) ln \frac{1}{1 - \frac{(v_v - v_l)(B/v_v)/(B/v_v + 1/v_l)}{c_p(dp_v/dT_l)^{-1} - v_l}} \tag{A.14}$$

Eq. (A.14) can be simplified to obtain an approximate relationship like Eq. (A.4). Eq. (A.14) is written as an exponential function, and $c_p\,(dp_v/dT_l)^{-1} - v_l \approx c_p\,(dp_v/dT_l)^{-1}$ and $(B/v_v)\,/(B/v_v + 1/v_l) \approx Bv_l/v_v$ are held because of $v_l \approx 0$

$$e^{\frac{v_v \Delta p_v}{L}} = \frac{1}{1 - \frac{v_v B v_l/v_v}{c_p (dp_v/dT_l)^{-1}}} \tag{A.15}$$

Usually, $0 < v_v \Delta p_v/L < 1$, thus $e^{\frac{v_v \Delta p_v}{L}} \approx 1 + v_v \Delta p_v/L$; consequently, Eq. (A.15) is approximated as follows

$$\left(1 + \frac{v_v \Delta p_v}{L}\right)\left[1 - \frac{v_v B v_l/v_v}{c_p\,(dp_v/dT_l)^{-1}}\right] = 1 \tag{A.16}$$

Furthermore

$$1 + \frac{v_v \Delta p_v}{L} - \frac{v_v B v_l/v_v}{c_p\,(dp_v/dT_l)^{-1}} + \left(\frac{v_v \Delta p_v}{L}\right)\left[\frac{v_v B v_l/v_v}{c_p\,(dp_v/dT_l)^{-1}}\right] = 1 \tag{A.17}$$

The last term is in a 2nd-order small quantity owing to $0 < v_v B\,(v_v/v_l)\,/\left[c_p\,(dp_v/dT_l)^{-1}\right] < 1$, and it can be neglected naturally, then

$$\frac{\Delta p_v}{L} = \frac{B\,(v_l/v_v)}{c_p\,(dp_v/dT_l)^{-1}} \tag{A.18}$$

Clearly, Eq. (A.18) is identical to Eq. (A.4). Unfortunately, the combined variable $(v_v/v_l)\left(c_p/L\right)(dp_v/dT_l)^{-1}$ was with dimension and was called the thermal cavitation parameter B_t (Fisher et al., 1945). After the B is replaced with V_v/V_l, and $(v_v/v_l)\left(c_p/L\right)(dp_v/dT_l)^{-1}$ is denoted by B_t, The vapour pressure depression is expressed as

$$\Delta p_v = \frac{1}{B_t}\frac{V_v}{V_l},\ B_t = \frac{v_v}{v_l}\frac{c_p}{L}\left(\frac{dp_v}{dT_l}\right)^{-1} \tag{A.19}$$

In Spraker (1965), it was assumed that V_v/V_l is the same for all centrifugal pumps and liquids during cavitation at 3% head drop point, hence the NPSHr correction ΔNPSHr$(=\Delta p_v v_l/g)$ was a function of $1/B_t$. For pure liquids such as water, butane, methyl alcohol and Freon 11, ΔNPSHr can be correlated with $ln\,(1/B_t)$. For a mixture liquid, namely gasoline, crude oil and fuel oil, however, ΔNPSHr can be divided two parts, one part is correlated with $ln\,(1/B_t)$ and the part is related to liquid temperature pumped (Spraker, 1965).

Eq. (A.14) has been derived in Jacobs (1961) as well, but any ΔNPSHr correlations were not proposed even the suction performance of a single-stage submerged booster pump had been measured when pumping liquid hydrogen.

Based on factor $1/B_t$ and impeller Reynolds number, a correlation of NPSHr was proposed in Barenboim (1966) to fit the experimental NPSHr of various liquids in centrifugal pumps in Salemann (1959). Similarly, an empirical correlation of ΔNPSHr was developed for inducers in Shcherbatenko and Shapiro (1981) in terms factor $1/B_t$, Froude number, Weber number and Reynolds number of a wedge-shaped cavity in the blade suction side in the mean-line cascade. The coefficients in the correlation were best fitted with the experimental data of nine inducers. Effects of liquid viscosity and thermodynamics on the cavitation performance of centrifugal pumps were discussed but any correlations were not put forward (Shcherbatenko, 1982).

Two linear empirical correlations of NPSHr were proposed by employing an integrated variable, for instance $B_t^{-1}\,(\mathrm{PrRe})^{1/2}\left(\rho_{lref}/\rho_l\right)^{4/3}(p_v/p_a)\,\mathrm{Re}^m$, ρ_{lref} is density of the liquid at a reference temperature, p_a is atmosphere pressure, in terms of the experimental data on suction performance of centrifugal pumps in Salemann (1959) and Spraker (1965). These correlations read as (Chivers, 1969-70)

$$\mathrm{NPSHr} = aB_t^{-1}\,(\mathrm{PrRe})^{1/2}\left(\rho_{lref}/\rho_l\right)^{4/3}(p_v/p_a)\,\mathrm{Re}^m + b \tag{A.20}$$

where a, b are empirical constant determined by curve fitting, $m = 0.8$ for the experimental data in Salemann (1959) and Spraker (1965).

A.3. ΔT and B correlations

In the thermal analysis of cavitation above, the thermodynamic or energy balance equation was concerned only, i.e. the fluid is stationary with heat conduction, thus the convective heat transfer process has been overlooked in flows. To take this process into account, it was assumed that the velocity of vapour removal from the cavity by entrainment is proportional to the velocity of fluid flow in turbulent regime and the temperature depression in the cavity is written as (Holl and Wisclicenus, 1961)

$$\Delta T = C\frac{A_v}{A_l}\frac{v_l}{v_v}\frac{L}{c_p}\mathrm{Pe} \tag{A.21}$$

where A_v, A_v are areas of vapour removal and heat supply through the liquid, Pe is the ratio of heat transfer by convection to that by conduction, i.e. the Peclet number, $\mathrm{Pe} = c_p VD/kv_l$, V and D are the characteristic velocity of the liquid and the characteristic dimension of the pump impeller, k is the heat conductivity of the liquid, C is experimental constant. Once a ΔT is available, the pressure depression can be calculated via $\Delta p_v = dp_v/dT_l \Delta T$.

Another proposal of ΔT was raised in Acosta and Parkin (1961). The chief contribution is to include Reynolds number Re, Prandtl number Pr and Froude number Fr into the constant C, namely

$$\Delta T = \frac{C_Q}{C_H}\frac{A_v}{A_l}\frac{v_l}{v_v}\frac{L}{c_p} \tag{A.22}$$

where $C_H = C_H\,(\mathrm{Re}, \mathrm{Pr}, \mathrm{Fr})$ is the empirical heat transfer coefficient, $C_Q = C_Q\,(\mathrm{Re}, \mathrm{Fr})$ is the liquid volume entrainment coefficient or flow coefficient. For pumps Fr does not play a role. By using the Clausius–Clapeyron equation, Eqs. (A.6), (A.22) is updated to the following

$$\Delta p_v = \frac{C_Q}{C_H}\frac{A_v}{A_l}\frac{v_l}{v_v}\frac{1}{\left(1 - \frac{v_l}{v_v}\right)}\frac{L^2}{v_v c_p T_l} \tag{A.23}$$

A similar piece of work was found in Holl et al. (1975), where the heat balance between the energy required in vaporization process and the heat transfer through the cavity boundary surface was established, such as

$$L\,(Q_v/v_v) = h_f A_{surf}\,(T_l - T_v) = h_f A_{surf}\,\Delta T \tag{A.24}$$

where Q_v is volume flow rate of the vapour, h_f is the film heat transfer coefficient, A_{surf} is the cavity surface area.

Expressing Q_v with the flow rate coefficient C_Q, and characteristic flow velocity V and pump impeller dimension D, $Q_v = C_Q D^2 V$, then ΔT can be written as the following based on Eq. (A.24)

$$\Delta T = \frac{C_Q}{h_f}\frac{D^2}{A_{surf}}\frac{VL}{v_v} \tag{A.25}$$

Eq. (A.25) is formulated in terms of nondimensional coefficients or numbers, that is

$$\Delta T = \frac{C_Q}{C_A}\frac{\mathrm{Pe}}{\mathrm{Nu}}\frac{v_l}{v_v}\frac{L}{c_p} \tag{A.26}$$

where C_A is area coefficient, $C_A = A_{surf}/D^2$, Pe is the Peclet number, $\mathrm{Pe} = VD/\alpha$, α is thermal diffusivity of the liquid,

$\alpha = k/(\rho_l c_p)$, measuring the rate of heat transfer of a material from the hot end to the cold end, Nu is the Nusselt number, $\mathrm{Nu} = h_f D/k$, meaning the ratio of convective to conductive heat transfer at a boundary in a fluid. The empirical correlations of C_A with D_c/D, C_Q with Re, Fr, D_c/D and Nu with Re, Fr, Pr, D_c/D were proposed according to previous cavitation tests on quarter- and zero-calibre ogives in Holl and Wisclicenus (1961). Effects of liquid surface tension on C_Q and Nu was clarified by introducing the Weber number, $\mathrm{We} = V\sqrt{D}/\sqrt{\varsigma/\rho_l}$, where ς is surface tension of the liquid, based on the experimental cavitation data in quarter- and zero-calibre ogives and Venturis (Holl et al., 1975). A survey of empirical ΔT was made in Bonnin et al. (1981). A C_Q empirical correlation was developed based on Venturi cavitation test in Fruman et al. (1999).

Experiments were performed in four-bladed inducer as pumping refrigerant R114 and B-factor was correlated to C_Q, Re and Pr (Franc et al., 2004). The corresponding correlation reads as

$$B = C_Q \mathrm{Re}^{0.2}\mathrm{Pr}^{0.7} \tag{A.27}$$

where $C_Q = \sqrt{\ell/c}$, ℓ is cavity length over a blade of the inducer, c is chord length of the blade.

Those studies suggest that it is impossible to predict ΔT and Δp_v accurately based on any theoretical thermodynamic or heat transfer models. Empirical correlations must be established and utilized by making use of existing experimental cavitation data to bridge the gap.

A.4. General B factor correlations

Refrigerant Freon 114 or R114 was applied to a specially designed Venturis to investigation into cavitation similarity in terms of thermodynamic effect expressed by measured vapour pressure and temperature depressions in Gelder et al. (1966). Firstly, a cavitation number for describing the similarity of developed cavitation in a Venturi was put forward based on the far field pressure p_∞ and velocity V_∞ of a liquid at the inlet of a Venturi, and the vapour pressure in the cavity $p_v(T_v)$, namely

$$\begin{aligned}\sigma_v(T_v) &= \frac{p_\infty - p_v(T_v)}{\frac{1}{2}\rho_l V_\infty^2} = \frac{p_\infty - p_v(T_l)}{\frac{1}{2}\rho_l V_\infty^2} + \frac{p_v(T_l) - p_v(T_v)}{\frac{1}{2}\rho_l V_\infty^2} \\ &= \sigma_l(T_l) + \frac{\Delta p_v}{\frac{1}{2}\rho_l V_\infty^2}\end{aligned} \tag{A.28}$$

where $\sigma_v(T_v)$ is the cavitation number with thermodynamic effect at vapour temperature T_v, $\sigma_l(T_l)$ is the cavitation number without thermodynamic effect at liquid temperature T_l, $\sigma_l(T_l) = [p_\infty - p_v(T_l)]/\frac{1}{2}\rho_l V_\infty^2$, Δp_v is the vapour pressure depression due to the vapour pressure drop in the cavity, $\Delta p_v = p_v(T_l) - p_v(T_v)$. If $\sigma_v(T_v)$ of liquid flow systems keeps constant, then the developed cavitation in them with thermodynamic effect will have a similarity. Obviously, Δp_v must be known in advance to gain the $\sigma_v(T_v)$ in a liquid flow system.

Secondly, the criterion B in Eq. (A.7) is in the following empirical correlation based on the experimental data for R114 (Gelder et al., 1966)

$$B = B_{ref}\left(\frac{\alpha}{\alpha_{ref}}\right)^{-0.5}\left(\frac{D_c}{D_{cref}}\right)^{0.16}\left(\frac{V_\infty}{V_{\infty ref}}\right)^{0.85} \tag{A.29}$$

where B_{ref}, D_{cref} and $V_{\infty ref}$ are known reference B, α, D_c and V_∞, respectively. If α, D_c and V_∞ are available, then B can be determined with Eq. (A.29). Finally, Δp_v and $\sigma_v(T_v)$ will be calculated from Eqs. (A.7) and (A.28). In Moor and Ruggeri (1968a), the exponent 0.16 for R114 in Eq. (A.29) is 0.15. In Moor and Ruggeri (1968b), the empirical correlation of B for both liquid-hydrogen and R114 is slightly different from Eq. (A.29), i.e.

$$B = B_{ref}\left(\frac{\alpha}{\alpha_{ref}}\right)^{-1.0}\left(\frac{D_c/D}{D_{cref}/D_{ref}}\right)^{0.3}\left(\frac{D}{D_{ref}}\right)^{0.2}\left(\frac{V_\infty}{V_{\infty ref}}\right)^{0.80} \tag{A.30}$$

where D and D_{ref} are the inlet diameters of the current and reference Venturis, respectively.

Eq. (A.30) is applicable to centrifugal pumps as well. In industry, NPSHr is generally calculated by using the liquid–vapour pressure at a liquid pumping temperature T_l. In this context, the NPSHr is expressed as (Ruggeri and Moor, 1969; Hord, 1974)

$$\mathrm{NPSHr}(T_l) = \frac{p_\infty}{\rho_l g} + \frac{V_\infty^2}{2g} - \frac{p_v(T_l)}{\rho_l g} \tag{A.31}$$

where the pressure p_∞ and the pressure p_∞ and velocity V_∞ of the liquid at the inlet of a pump impeller. $\mathrm{NPSHr}(T_l)$ of a pump is very commonly measured in a pump manufacturer's laboratory by using cold water without thermodynamic effect during cavitation test. When the pump is used to transport hot water or hydrocarbon or refringent, the $\mathrm{NPSHr}(T_l)$ of the pump at that liquid pumped temperature can differ from that of cold water due to the thermodynamic effect in the cavitation of that liquid.

Eq. (A.28) states that the vapour temperature based $\sigma_v(T_v)$ is the factor for determining cavitation similarity with thermodynamic effect and should remain unchanged at a similar operating point in geometrically similar pumps. From Eq. (A.31), $\sigma_l(T_l)$ is expressed in terms of $\mathrm{NPSHr}(T_l)$ in the following form

$$\sigma_l(T_l) = \frac{\mathrm{NPSHr}(T_l)}{\frac{V_\infty^2}{2g}} - 1 \tag{A.32}$$

Substituting Eq. (A.32) into Eq. (A.28) for $\sigma_l(T_l)$, then $\sigma_v(T_v)$ in terms of $\mathrm{NPSHr}(T_l)$ and Δp_v arrives at

$$\begin{aligned}\sigma_v(T_v) &= \left[\frac{\mathrm{NPSHr}(T_l)}{\frac{V_\infty^2}{2g}} - 1\right] + \frac{\Delta p_v}{\frac{1}{2}\rho_l V_\infty^2} \\ &= \left[\frac{\mathrm{NPSHr}(T_l) + \Delta p_v/\rho_l g}{\frac{V_\infty^2}{2g}}\right] - 1\end{aligned} \tag{A.33}$$

Under current and reference conditions, $\sigma_v(T_v) = \sigma_{vref}(T_v)$, and $V_\infty/V_{\infty ref} = nD/n_{ref}D_{ref}$, where n and n_{ref} are the current and reference rotative speeds of the geometrically similar pumps at similar operating points, then based on Eq. (A.33), the similarity in $\mathrm{NPSHr}(T_l) + \Delta p_v/\rho_l g$ is expressed as

$$\frac{\mathrm{NPSHr}(T_l) + \Delta p_v/\rho_l g}{\mathrm{NPSHr}(T_l)_{ref} + (\Delta p_v/\rho_l g)_{ref}} = \left(\frac{nD}{n_{ref}D_{ref}}\right)^2 \tag{A.34}$$

If $\mathrm{NPSHr}(T_l)_{ref}$, $(\Delta p_v/\rho_l g)_{ref}$, n_{ref}, $\Delta p_v/\rho_l g$ and n are known in prior, then the current $\mathrm{NPSHr}(T_l)$ is predicted with the expression

$$\begin{aligned}\mathrm{NPSHr}(T_l) = \left(\frac{nD}{n_{ref}D_{ref}}\right)^2 &\left[\mathrm{NPSHr}(T_l)_{ref} + (\Delta p_v/\rho_l g)_{ref}\right] \\ &- \Delta p_v/\rho_l g\end{aligned} \tag{A.35}$$

To work out $\Delta p_v/\rho_l g$, Eqs. (A.30) and (A.7) should be utilized. It is assumed that the dimensionless cavity D_c/D remains essentially constant for various liquids, liquid temperatures and rotative speeds, and letting $V_\infty/V_{\infty ref} = nD/n_{ref}D_{ref}$ once again, then Eq. (A.30) is simplified as follows

$$B = B_{ref}\left(\frac{\alpha}{\alpha_{ref}}\right)^{-1.0}\left(\frac{D}{D_{ref}}\right)^{0.2}\left(\frac{nD}{n_{ref}D_{ref}}\right)^{0.80} \tag{A.36}$$

For the same pump, $D/D_{ref} = 1$, Eq. (A.36) can become even simpler form. Since B_{ref} and $(\Delta p_v/\rho_l g)_{ref}$ must be known initially, two sets of experimental data should be utilized to determine B_{ref} and $(\Delta p_v/\rho_l g)_{ref}$ iteratively, then one can predict NPSHr (T_l) under any other conditions with them. This is a drawback of the method even though it has found applications to hydrogen (Ruggeri and Moor, 1969; Meng, 1968) and butane (Ruggeri and Moor, 1969) and hot water (Kovich, 1972; Manabe and Miyagawa, 2006).

The mechanism of head breakdown in cavitating inducers was associated with the Mach number of the liquid–vapour two-phase flow in the cavity (Jakobsen, 1964), especially, when the Mach number is unity, $M = 1$, the flow passages of inducer were choked. The Mach number is related to the characteristic velocity V_∞, liquid sound speed a_l, vapour sound speed a_v, B factor, liquid specific volume v_l and vapour specific volume v_v, and expressed by using the following expression (Hord, 1974)

$$M = \frac{V_\infty}{a_l}\sqrt{\frac{1 + B\,(v_v/v_l)\,(a_l/a_v)^2}{1 + B\,(v_l/v_v)}} \tag{A.37}$$

M was used to correlate to experimental B factor by replacing V_∞ in Eq. (A.30), and the corresponding the correlation is written as (Hord, 1974)

$$B = B_{ref}\left(\frac{\alpha}{\alpha_{ref}}\right)^{-1.0}\left(\frac{D_c/D}{D_{cref}/D_{ref}}\right)^{0.28}\left(\frac{D}{D_{ref}}\right)^{0.71}\left(\frac{M}{M_{ref}}\right)^{0.51} \tag{A.38}$$

Since B factor has been involved in M expression, Eq. (A.38) is hard to be applied but also does not show any improvement in prediction accuracy (Hord, 1974).

A.5. Method of characteristic temperature depression ΔT^+

A characteristic temperature depression-based approach was put forward in Zika (1984). According to Eq. (A.19),

$$\Delta p_v = \frac{B}{B^\circ}\frac{dp_v}{dT_l}, B^\circ = \frac{v_v}{v_l}\frac{c_p}{L} \tag{A.39}$$

where factor B° is the volume ratio corresponding to a unit temperature drop. The ratio B/B° is with temperature unit and is named as characteristic temperature depression ΔT^+, which is a function of liquid thermodynamic property only. It was illustrated that ΔT^+ $(=B/B^\circ)$ data of water, benzene, butane, Freon 11 and methanol collapse onto a single curve in terms of their corrected vapour pressure p_v^{cor} (the actual vapour pressure minus the vapour pressure of water at 20 °C). This means that ΔT^+ can serve as the similarity parameter for cavitation with thermodynamic effect in a pump, i.e. the following expression is held

$$\Delta p_v\frac{dT_l}{dp_v} = \frac{B}{B^\circ} = \Delta T^+ = f_1\left(p_v^{cor}\right) \tag{A.40}$$

It was hypothetical that after the vapour pressure depression Δp_v is replaced with NPSHr Eq. (A.40) is still true (Zika, 1984). Then NPSHr can be correlated to ΔT^+ with

$$\text{NPSHr}\frac{dT_l}{dp_v} = const \times \Delta T^+ = f_2\left(p_v^{cor}\right) \tag{A.41}$$

Finally, NPSHr will be related to the ratio of ΔT^+ to dT_l/dp_v, that is

$$\text{NPSHr} = const \times \frac{\Delta T^+}{\frac{dT_l}{dp_v}} = f_3\left(p_v^{cor}\right) \tag{A.42}$$

Eq. (A.42) was applied to correlated NPSHr-p_v curve of six centrifugal pumps tested in Spraker (1965). Since the number of examples is too few, the method of Zika (1984) does not exhibit a distinctly better accuracy than that in Stepanoff (1964). The approach does not seem to offer a resolution in correction of NPSHr of cold water to obtain the NPSHr of a liquid other than water.

A.6. Σ factor method

The compressibility of cavitation bubbles was analysed at the inlet of an inducer in terms of the Rayleigh–Plesset equation with thermodynamic effect; particularly, a criterion determining boiling driven by temperature increase and cavitation owing to pressure reduction in a pump impeller was established (Brennen, 1973). The criterion was described with a dimensional thermodynamic parameter Σ and an impeller cavitation performance variable Λ. The criterion is presented as follows

$$\begin{cases} \Sigma = \dfrac{L^2 v_l^2}{T_l c_p v_v^2\sqrt{\alpha}},\ \Lambda = \left(\dfrac{V_\infty^3\sigma_l}{D}\right)^{1/2} \\ \Lambda < \Sigma,\ \text{boiling} \\ \Lambda > \Sigma,\ \text{cavitation} \end{cases} \tag{A.43}$$

In boiling state, the liquid temperature keeps unchanged, and there is not thermodynamic effect. In the cavitation state, however, the thermodynamic effect occurs and the liquid temperature is changed during cavitation. According to this fact, a Σ and Λ based method was developed in Arakeri (1999) to predict NPSHr (T_l) of hot water or hydrocarbons or refrigerans or cryogens. The method is in the following procedure:

(1) Determine a appreciate liquid temperature T_l^* with the condition $\Lambda = \Sigma$ for a given pump and liquid pumped with the known V_∞, σ_l and D;

(2) If the pump operating liquid temperature yields $T_l \le T_l^*$, then there is no thermodynamic effect in cavitation, NPSHr (T_l) has not a need of correction;

(3) If the temperature is in line with $T_l > T_l^*$, NPSHr (T_l) needs a correction. The NPSHr (T_l) experimental data in Salemann (1959), Stepanoff (1961) and Spraker (1965) were reprocessed by Arakeri (1999) and the correction ΔNPSHr was correlated to the reduced temperature T_R $[=(T_l - T_l^*)/(T_c - T_l^*)]$, T_c is the critical temperature of the liquid. The ΔNPSHr $- T_R$ curves and the corresponding scattered experimental data are illustrated in Fig. 3.

ΔNPSHr is the NPSHr correction to a pump at fixed rotative speed and impeller diameter as well as the same working point, meaning $nD/n_{ref}D_{ref} = 1$. Consequently, (Eqn (A.35)) is simplified to the following form

$$\text{NPSHr}\,(T_l) + \Delta p_v/\rho_l g = \text{NPSHr}\,(T_l)_{ref} + (\Delta p_v/\rho_l g)_{ref} \tag{A.44}$$

Letting $\Delta\text{NPSHr} = \Delta p_v/\rho_l g - (\Delta p_v/\rho_l g)_{ref}$, the relationship between NPSHr (T_l) and NPSHr $(T_l)_{ref}$ is established as follows

$$\text{NPSHr}\,(T_l) = \text{NPSHr}\,(T_l)_{ref} - \Delta\text{NPSHr} \tag{A.45}$$

If one knows NPSHr $(T_l)_{ref}$ of a liquid at a temperature, then ΔNPSHr of the liquid at another temperature can be figured out, finally one can predict NPSHr (T_l) of that liquid at that temperature. Usually, NPSHr $(T_l)_{ref}$ is for cold water in industry, and ΔNPSHr is for a liquid other than water, then Eq. (A.45) allows one to have NPSHr (T_l) of that liquid. Since it yields $\Delta\text{NPSHr} \ge 0$, NPSHr (T_l) of that liquid is always smaller than NPSHr $(T_l)_{ref}$ of cold water. This fact implies that a pump is subject to a lowered NPSHr when pumping hot water, hydrocarbons or refrigerants or cryogens compared with that when handling cold water.

Similarly, Z factor was proposed to describe thermodynamic effect in sheet cavitation over a hydrofoil (Kato, 1984), i.e.

$$Z = C_z \frac{L}{k}\sqrt{\frac{\alpha v_l}{v_v}}\frac{dp_v}{dT_l} = C_z\sqrt{\frac{v_v}{v_l}}\Sigma \tag{A.46}$$

Various factors for representing thermodynamic effect in cavitation were reviewed in Franc and Pellone (2007), Yoshida et al. (2008) and Yoshida et al. (2013). where C_z is experimental constant. Additionally, based on (Eqn (A.43)) and letting $\wedge = \Sigma$ and $V_\infty = \omega D$, where ω is pump impeller angular speed, D is impeller diameter, the following dimensionless parameter is resulted (Ehrlich and Murdock, 2015)

$$\sqrt{\sigma_l} = \frac{D\omega^{3/2}}{\Sigma} \tag{A.47}$$

in which $\sqrt{\sigma_l}$ was called the thermodynamic bubble growth parameter. $\sqrt{\sigma_l}$ decreases with increasing liquid temperature for inducers (Ehrlich and Murdock, 2015).

A.7. The Rayleigh–Plesset equation-based method

The formation and collapse of the individual cavitating bubbles around a cylindrical body with 1.5-caliber ogive nose in a water tunnel were studied by employing high-speed motion pictures up to 20,000 frames/second and the streamwise fluid pressure along the body wall was measured (Plessset, 1949). That fluid pressure profile was utilized to predict cavitating bubble growth and collapse in a variable fluid pressure field and compared with the observations made in Knapp and Hollander (1948), and the water temperature effect on the bubble growth and collapse was discussed quantitatively based on the conductive heat transfer equation between a spherical vapour bubble and its surrounding liquid. The work is a significant contribution to the very early work adhesive to constant fluid pressure condition in Rayleigh (1917).

The ideas about cavitating bubble growth and collapse and thermodynamic effect in Plessset (1949) were adopted and 1D numerical method for predicting cavitating bubble growth and collapse in a centrifugal pump impeller passage was put forwards in Grist (1986a) and Grist (1986b). The solved bubble growth and collapse 2nd-order differential equation i.e. Rayleigh–Plesset equation, has included bubble size change rate, number of bubbles, liquid surface tension, liquid thermal parameters, vapour and liquid volumetric flow rates, liquid pressure drop owing to cavity blockage, NPSH difference from cavitation inception, and pump non-cavitating head. The method can establish a relationship between bubble volumetric fraction and NPSH and predict pump head–NPSHa curve at different liquid temperatures for a specific centrifugal pump, but fail to develop empirical correlation for NPSHr based on experimental data of a variety of centrifugal pumps.

A.8. Empirical correlation for NPSH at cavitation inception

A theoretical model was built for estimating NPSH at cavitation inception in centrifugal pumps in Al-Arabi and Selim (2007). The NPSH at cavitation inception is written as

$$\mathrm{NPSH}_i = (1.04 + \sigma_b)\frac{v_{m1}^2}{2g} + \sigma_b\frac{u_1^2}{2g} + \frac{\Delta v_1^2}{2g} \tag{A.48}$$

where σ_b is the cavitation number, v_{m1} is the meridional absolute velocity of fluid at impeller inlet, u_1 is the tip speed of impeller inlet, Δv_1 is the change of the absolute velocity of fluid before and after the blade leading edge at impeller inlet. σ_b was correlated to thermodynamic effect in cavitation by using the method in Hord (1974), pump flow rate ratio, rotational speed ratio, and liquid temperature, v_{m1} and Δv_1 were related to pump flow rate ratio. The effect of non-condensable gas concentration on the cavitation threshold was considered. The model was validated by using 20 sets of experimental data of water at room or slightly high temperature (Al-Arabi and Selim, 2007). Whether the model is suitable for the liquids other than water is unknown.

References

Acosta, A.J., Parkin, B.R., 1961. Discussion on scale effects on cavitation. ASME J. Basic Eng. 83 (3), 395–396.

Al-Arabi, A.A., Selim, S.M., 2007. A theoretical model to predict cavitation inception in centrifugal Pumps. In: Proceedings of the 5th International Conference on Heat transfer, Fluid Mechanics and Thermodynamics(HEFAT2007), Paper No. AA2, Sun City, South Africa.

Arakeri, V.H., 1999. Contributions to some cavitation problems in turbomachinery. Sadhana 24 (6), 453–483.

Bala, E.J., O'Callaghan, P.W., Probert, S.D., 1985. Influence of organic working fluids on the performance of a positive-displacement pump with sliding vanes. Appl. Energy 20, 153–159.

Barenboim, A.B., 1966. Conditions for modelling cavitation phenomena in pumps for refrigeration liquids. B.H.R.A. Translation No. T865, (Russian original, 1965).

Bianchi, G., Fatigati, F., Murgia, S., et al., 2016. Modeling and experimental activities on a small-scale sliding vane pump for ORC-based waste heat recovery applications. Energy Procedia 101, 1240–1247.

Bollina, E., 1984. Head-flow and npsh performance of an axial piston pump working with organic fluids at different temperatures. Int. J. Heat Fluid Flow 5 (2), 93–100.

Bonnin, J., Billet, M.L., Hammitt, F.G., et al., 1981. Survey of present knowledge on cavitation in liquids other than cold water. J. Hydraul. Res. 19 (4), 277–305.

Borsukiewicz-Gozdur, A., 2013. Pumping work in the organic rankine cycle. Appl. Therm. Eng. 51, 781–786.

Brennen, C., 1973. The dynamic behaviour and compliance of a stream of cavitating bubbles. ASME J. Fluids Eng. 95 (4), 533–541.

Casari, N., Fadiga, E., Pinelli, M., et al., 2019. Pressure pulsation and cavitation phenomena in a micro-ORC system. Energies 12, 2186.

Chang, J.C., Hung, T.C., He, Y.L., et al., 2015. Experimental study on low-temperature organic rankine cycle utilizing scroll type expander. Appl. Energy 155, 150–159.

Chen, H.J., Goswami, D.Y., Stefanakos, E.K., 2010. A review of thermodynamic cycles and working fluids for the conversion of low-grade heat. Renew. Sustain. Energy Rev. 14, 3059–3067.

Chivers, T.C., 1969-70. The correlation of cavitating performance for a centrifugal pump handling various liquids. Proc. IMechE-Part 1 184 (2), 48–56.

Colonna, P., Casati, E., Trapp, C., et al., 2015. Organic rankine cycle power systems: from the concept to current technology, applications, and an outlook to the future. ASME J. Eng. Gas Turbines Power 137 (10), 100801, (19 pages).

D'Amico, F., Pallis, P., Leontaritis, A.D., et al., 2018. Semi-empirical model of a multi-diaphragm pump in an organic rankine cycle (ORC) experimental unit. Energy 143, 1056–1071.

Deniau, P., 2009. Applying NPSH to metering pumps. World Pumps (8), 34–37.

Ehrlich, D.A., Murdock, J.W., 2015. A dimensionless scaling parameter for thermal effects on cavitation in turbopump inducers. ASME J. Fluids Eng. 137 (4), 1–8.

Fisher, R.C., et al., 1945. Communications on a survey of modern centrifugal pump practice for oilfield and refinery services. Proc. IMechE 152 (1), 303–314.

Franc, J., Pellone, C., 2007. Analysis of thermal effects in a cavitating inducer using Rayleigh equation. ASME J. Fluids Eng. 129 (8), 974–983.

Franc, J.P., Rebattet, C., Coulon, A., 2004. An experimental investigation of thermal effects in a cavitating inducer. ASME J. Fluids Eng. 126 (5), 716–723.

Fruman, D.H., Reboud, J., Stutz, B., 1999. Estimation of thermal effects in cavitation of thermosensible liquids. Int. J. Heat Mass Transfer 42 (17), 3195–3204.

Gao, P., Wang, L.W., Wang, R.Z., et al., 2015. Experimental investigation on a small pumpless ORC (organic rankine cycle) system driven by the low temperature heat source. Energy 91, 324–333.

Gelder, T.F., Ruggeri, R.S., Moor, R.D., 1966. Cavitation similarity considerations based in measured pressure and temperature depressions in cavitated regions of Freon 114. NASA TN D-3509.

Griffiths, D.V., Smith, I.M., 1991. Numerical Methods for Engineers. Blackwell Scientific Publications Ltd, Oxford, pp. 219–231.

Grist, E., 1986a. The volumetric performance of cavitating centrifugal pumps part 1: theoretical analysis and method of prediction. Proc. Inst. Mech. Eng. Part A 200 (3), 159–167.

Grist, E., 1986b. The volumetric performance of cavitating centrifugal pumps part 2: predicted and measured performance. Proc. Inst. Mech. Eng. Part A 200 (3), 168–172.

Holl, J.W., Billet, M.L., Weir, D.S., 1975. Thermodynamic effects on developed cavitation. ASME J. Fluids Eng. 97 (4), 507–513.
Holl, J.W., Wisclicenus, G.F., 1961. Scale effects on cavitation. ASME J. Basic Eng. 83 (3), 385–395.
Hord, J., 1974. Cavitation in Liquid Cryogens-IV: Combined Correlations for Venturi, Hydrofoil, Ogives and Pumps. NASA CR-2448.
Idelchik, I.E., 1966. Handbook of Hydraulic Resistance. Israel Program for Scientific Translations Ltd., p. 370.
Jacobs, R.B., 1961. Prediction of symptoms of cavitation. J. Res. Nat. Bur. Stand.-Eng. Instrum. 65C (3), 147–156.
Jakobsen, J.K., 1964. On the mechanism of head breakdown in cavitating inducers. ASME J. Fluids Eng. 86 (2), 291–305.
Kaczmarczyk, T.Z., Żywica, G., Ihnatowicz, E., 2016. Experimental Investigation on a Rotodynamic Pump Operating in the Cogeneration System with a Low-Boiling Working Medium, Vol. 134. Transactions of Institute of Fluid-Flow Machinery, pp. 63–87.
Kato, H., 1984. Thermodynamic effect on incipient and developed sheet cavitation. In: Proceedings of International Symposium on Cavitation Inception, FED-Vol. 16. pp. 127–136.
Knapp, R.T., Hollander, A., 1948. Laboratory investigations of the mechanism of cavitation. Trans. ASME 70, 419–435.
Kovich, G., 1972. Experimental and Predicted Cavitation Performance of 80.6° Helical Inducer in High-Temperature Water. NASA TN D-6809.
Landelle, A., Tauveron, N., Haberschill, P., et al., 2015. Study of reciprocating pump for supercritical ORC at full and part load operation. In: Proceedings of the 3rd International Seminar on ORC Power Systems (ASME ORC 2015), 12-14 October, Brussels, Belgium.
Landelle, A., Tauveron, N., Revellin, R., et al., 2017. Performance investigation of reciprocating pump running with organic fluid for organic Rankine cycle. Appl. Therm. Eng. 113, 962–969.
Lee, J.K., Jung, J.K., Chai, J.B., et al., 2015. Mathematical modelling of reciprocating pump. J. Mech. Sci. Technol. 29 (8), 3141–3151.
Manabe, J., Miyagawa, K., 2006. High temperature NPSH and its application for feedwater system. JSME Int. J.-Ser. B 49 (2), 352–359.
Meng, P.R., 1968. Change in Inducer Net Positive Suction Head Requirement with Flow Coefficient in Low Temperature Hydrogen (27.9° to 36.6° R). NASA TN D-4423.
Moor, R.D., Ruggeri, R.S., 1968a. Venturi scaling studies on thermodynamic effects of developed cavitation of Freon-114. NASA TN D-4387.
Moor, R.D., Ruggeri, R.S., 1968b. Prediction of thermodynamic effects of developed cavitation based on liquid-hydrogen and Freon-114 data in scaled Venturis. NASA TN D-4899.
Opitz, K., Schade, O., Schlücker, E., 2011. Cavitation in reciprocating positive displacement pumps. In: Proceedings of 27th International Pump Users Symposium. Turbomachinery Laboratories, Texas A & M University, USA, pp. 27–33.
Opitz, K., Schlücker, E., 2010. Detection of cavitation phenomena in reciprocating pumps using a high-speed camera. Chem. Eng. Technol. 33 (10), 1610–1614.
Park, B.S., Usman, M., Imran, et al., 2018. Review of organic rankine cycle experimental data trends. Energy Convers. Manage. 173, 679–691.
Parry, W.W., 1986. System problem experience in multiple reciprocating pump installations. In: Proceedings of 3rd International Pump Users Symposium. Turbomachinery Laboratories, Texas A & M University, USA, pp. 21–25.
Plessset, M.S., 1949. The dynamics of cavitation bubbles. ASME J. Appl. Mech. 16 (3), 277–282.
Quoilin, S., VanDenBroek, M., Declaye, S., 2013. Techno-economic survey of organic rankine cycle (ORC) systems. Renew. Sustain. Energy Rev. 22, 168–186.
Rahbar, K., Mahmoud, S., Al-Dadah, R.K., et al., 2015. Modelling and optimization of organic rankine cycle based on a small-scale radial inflow turbine. Energy Convers. Manage. 91, 186–198.
Rayleigh, O.M., 1917. On the pressure developed in a liquid during the collapse of a spherical cavity. London, Edinburgh, Dublin Phil. Mag. J. Sci. Ser. 6 34 (200), 94–98.
Richardson, E.S., 2016. Thermodynamic performance of new thermofluidic feed pumps for organic rankine cycle applications. Appl. Energy 161, 75–84.
van Rijswick, R., Talmon, A., van Rhee, C., 2016. Fluid–structure interaction (FSI) in piston diaphragm pumps. Canad. J. Chem. Eng. 94 (6), 1116–1126.
Ruggeri, R.S., Moor, R.D., 1969. Method for Prediction of Pump Cavitation Performance for Various Liquids, Liquid Temperatures, and Rotative Speeds. NASA TN D-5292.
Sahoo, T., 2006. Cavitation in reciprocating pumps. World Pumps (1), 24–27.
Salemann, V., 1959. Cavitation and NPSH requirements of various fluids, 81 (2), 167-173.
Sanger, N.L., 1968. Cavitating performance of two low-area-ratio water jet pumps having throat lengths of 7.25 diameters. NASA TN D- 4592, pp. 1–37.
Shcherbatenko, L.E., 1982. Determination of the cavitation characteristics of vane pumps in the presence of a scale effect. Chem. Pet. Eng. 18, 16–20.
Shcherbatenko, L.E., Shapiro, A.S., 1981. Influence of thermodynamic effect on cavitation in screw and screw centrifugal pumps. Chem. Pet. Eng. 17, 415–421.
Shu, G., Yu, Z., Liu, P., et al., 2018. Potential of a thermofluidic feed pump on performance improvement of the dual-loop rankine cycle using for engine waste heat recovery. Energy Convers. Manage. 171, 1150–1162.
Singh, P.J., Able, S.D., 1996. Determination of NPSHR for reciprocating positive displacement pumps: a new approach. In: Proceedings of 13th International Pump Users Symposium. Turbomachinery Laboratories, Texas A & M University, USA, pp. 131–139.
Spraker, W.A., 1965. The effects of fluid properties on cavitation in centrifugal pumps. ASME J. Eng. Power 87 (2), 309–318.
Stahl, H.A., Stepanoff, A.J., 1956. Thermodynamic aspects of cavitation in centrifugal pumps. Trans. ASME 78 (8), 1691–1693.
Stepanoff, A.J., 1961. Cavitation in centrifugal pumps with liquids other than water. ASME J. Eng. Power 83 (1), 79–89.
Stepanoff, A.J., 1964. Cavitation properties of liquids. ASME J. Eng. Power 86 (2), 195–199.
Tchanche, B.F., Pétrissans, M., Papadakisc, G., 2014. Heat resources and organic Rankine cycle machines. Renew. Sustain. Energy Rev. 39, 1185–1199.
Usman, M., Imran, Park, B.S., et al., 2015. Multi-objective optimization of evaporator of organic rankine cycle (ORC) for low temperature geothermal heat source. Appl. Therm. Eng. 80, 1–9.
Vetter, G., Schlucker, E., Horn, W., et al., 1995. Diaphragm development trends for safe leakage for reciprocating process pumps. In: Proceedings of 12th International Pump Users Symposium. Turbomachinery Laboratories, Texas A & M University, USA, pp. 207–230.
Vetter, G., Schweinfuter, F., 1987. Pressure pulsations in the piping of reciprocating pumps. Chem. Eng. Technol. 10, 262–271.
Vetter, G., Thiel, E., Stork, U., 1989. Reciprocating pump valve design. In: Proceedings of 6th International Pump Users Symposium. Turbomachinery Laboratories, Texas A & M University, USA, pp. 39–52.
Wachel, J.C., Tison, J.D., Price, S.M., 1989. The Effect of Pulsations on Cavitation in Reciprocating Pump Systems. ASME Paper 89-Pet-10, pp. 1–11.
Wang, X., Feng, Y.Q., Hung, T.C., 2020. Investigating the system behaviors of a 10kW organic Rankine cycle (ORC) prototype using plunger pump and centrifugal pump. Energies 13 (5), 1141.
White, F.M., 2011. Fluid Mechanics, 7th edition McGraw Hill, New York, p. 491.
Wu, M., Yue, X., Li, Y., et al., 2019. Design and analysis on the flow fluctuation of a new horizontal space multiphase crankshaft pump. J. Eng. 2019 (13), 159–162.
Yamada, N., Watanabe, M., Hoshi, A., et al., 2013. Experiment on pumpless rankine-type cycle with scroll expander. Energy 49, 137–145.
Yang, X.F., Xu, J.L., Miao, Z., et al., 2015. Operation of an organic rankine cycle dependent on pumping flow rates and expander torques. Energy 90, 864–878.
Yang, Y.X., Zhang, H.G., Tian, G.H., et al., 2019. Performance analysis of a multistage centrifugal pump used in an organic Rankine cycle (ORC) system under various condensation conditions. J. Therm. Science 28 (4), 621–634.
Yang, Y.X., Zhang, H.G., Xu, Y.H., et al., 2018. Matching and operating characteristics of working fluid pumps with organic Rankine cycle system. Appl. Therm. Eng. 142, 622–631.
Yoshida, Y., Kikuta, K., Watanabe, M., Hasegawa, S., et al., 2013. Effect of Thermodynamic Parameter on Cavitation in Rocket Inducer, JAXA Research and Development Memorandum, JAXA-RM-12-006E. Japan Aerospace Exploration Agency, pp. 1–25.
Yoshida, Y., Watanabe, M., Hasegawa, S., et al., 2008. Overview of Experimental Results of Cryogenic Inducer in JAXA, JAXA Research and Development Memorandum, JAXA-RM-08-005. Japan Aerospace Exploration Agency, pp. 1–10.
Zika, V.J., 1984. Correlation of cavitating centrifugal pumps. ASME J. Fluids Eng. 106 (2), 141–146.